Journal of Materials Chemistry A

ROYAL SOCIETY OF CHEMISTRY

REVIEW

View Article Online
View Journal | View Issue

Cite this: J. Mater. Chem. A, 2022, 10, 1682

Synthetic solid oxide sorbents for CO_2 capture: state-of-the art and future perspectives

Ribooga Chang, †[a] Xianyue Wu,†[bc] Ocean Cheung *[a] and Wen Liu *[b]

Carbon capture is an important and effective approach to control the emission of CO_2 from point sources such as fossil fuel power plants, industrial furnaces and cement plants into the atmosphere. For an efficient CO_2 capture operation, many aspects of the CO_2 capture steps need to be carefully considered. Currently the most mature CO_2 capture technology is liquid amine scrubbing. Alternatively, solid sorbents can be used to effectively capture CO_2 while alleviating the disadvantages associated with liquid amine sorbents. In this review, we critically assess solid metal oxide CO_2 sorbents, especially oxides of group 1 (Li, Na and K) and group 2 (Mg, Ca, Sr and Ba) metals, for capturing CO_2 at moderate to high temperatures. In particular, we focus on the recent advances in developing synthetic metal oxide sorbents, and the correlation between the design, synthetic approaches and their cyclic CO_2 capture performance, which are characterised by CO_2 uptake capacity, rate of carbonation and cyclic stability. The state-of-the-art, challenges, opportunities and future research directions for these metal oxide sorbents are discussed. By devoting more research effort to address the issues identified, there can be great potential to utilise Group 1 and 2 metal oxides as cost-effective, highly efficient sorbents for CO_2 capture in a variety of carbon capture applications.

Received 7th September 2021
Accepted 19th December 2021

DOI: 10.1039/d1ta07697c

rsc.li/materials-a

[a]Department of Materials Science and Engineering, Nanotechnology and Functional Materials, Uppsala University, SE75121, Sweden. E-mail: ocean.cheung@angstrom.uu.se

[b]School of Chemical and Biomedical Engineering, Nanyang Technological University, 62 Nanyang Drive, 637459, Singapore. E-mail: wenliu@ntu.edu.sg

[c]Interdisciplinary Graduate Programme, Nanyang Environmental & Water Research Institute, 1 Cleantech Loop, 637141, Singapore

† These authors contributed equally to this work.

Ribooga Chang is a PhD student at the Department of Materials Science and Engineering at Uppsala University, Sweden. Ribooga holds a master's degree from Gwangju Institute of Science and Technology (GIST), Korea. Her PhD work has been focused on the development of high-temperature sorbents and porous materials for a number of applications e.g. gas separation, water treatment, and drug delivery.

Xianyue Wu is a doctoral student in Chemical Engineering at the School of Chemical and Biomedical Engineering, Nanyang Technological University. Xianyue is also enrolled on an Interdisciplinary Graduate Programme in collaboration with Nanyang Environment & Water Research Institute (NEWRI), Residues, Resource and Reclamation Centre (R3C). She has a Bachelor of Engineering (Chemical and Biomolecular Engineering) with Honours (Highest Distinction) degree from Nanyang Technological University, Singapore. Her research interests include catalyst and process development in thermal catalysis of carbon monoxide and carbon dioxide. She is currently focusing on work regarding nickel-based dual function material for CO2 capture and conversion.

1 Introduction

1.1 Background

Global warming is one of the major challenges of the present century.[1] The high concentration of CO_2 in the atmosphere due to human activity is indisputably the main cause of global warming. In particular, the combustion of fossil fuels for electricity generation, transportation, oil refining, cement production and metallurgy results in the release of CO_2 into the atmosphere at a rate that is far beyond what the ecosystem can take up.[2] Therefore, decarbonisation technologies have been one of the focal points of research in science and engineering. In a sustainable and low-carbon future, renewable energies will eventually replace fossil fuels. In the meantime, the carbon capture, storage and utilisation scheme (CCSU) will play an important role as a transitional solution to provide low-emission hydrogen, electricity and CO_2-derived products from fossil fuel feedstocks. After renewable energies have completely decarbonised the energy sector, CCSU will continue to be relevant to industrial processes such as steelmaking and cement production.[3]

The first step in CCSU is the capture of CO_2 from point sources of emissions or, in the case of direct air capture (DAC), from the atmosphere. When capturing from the combustion of fossil fuels, three main strategies exist: pre-combustion, post-combustion and oxy-fuel combustion. Pre-combustion capture involves extracting CO_2 from syngas during hydrogen production (by gasification, reforming and downstream purification processes), followed by the combustion of the "blue hydrogen" produced. Post-combustion capture is an end-of-pipe strategy that extracts CO_2 from the combustion flue gases. Oxy-fuel combustion is proceeds by burning carbonaceous fuels in the absence of nitrogen. The flue gas of oxy-fuel combustion, after the removal of water, NO_x, SO_x and any residue N_2, can be considered captured. The interested reader is referred to Stanger *et al.*[4] for detailed discussions of various carbon capture strategies.

Regardless of the strategy, CO_2 capture requires gas separation, which can be achieved by various technologies including chemical scrubbing, physical adsorption (physisorption), cryogenic distillation, membrane separation, *etc.* Currently, chemical scrubbing using amine solutions is the most mature carbon capture technology, which can be deployed at commercially viable scales.[5] However, CO_2 capture by amine scrubbing is energy intensive (typically 4–6 MJ kg^{-1} CO_2 captured by monoethanolamine).[6] In addition, liquid amine solutions is expensive to produce, corrosive, and suffers from thermal and oxidative degradation during regeneration (although some priority amine formulations claim superior cyclic stability).[7]

Physical sorption processes utilise sorbents in either liquid form (*e.g.* selexol) or solid form (*e.g.* zeolites and metal–organic framework) and do not require high operating temperatures.[8,9] Instead, the regeneration of physical sorbents requires strong vacuum and/or gentle heating, which are associated with unrecoverable energy penalty. Physisorbents such as zeolites, zeotypes, metal–organic frameworks (MOFs) tend to perform best at ambient temperatures with respect to CO_2 uptake capacity: zeolites and zeotype typically have high CO_2 uptake at low pressures in the range of approximate 4–25 wt% up to 1 bar at ambient temperatures.[10] MOFs perform comparably better at high pressures, CO_2 uptake at ambient temperatures of well over 100 wt% have been reported close to the saturation pressure of CO_2 (*e.g.* NU-1000).[11,12] It is important to note that these physisorbents do not have high CO_2 uptake at high temperatures (*i.e.* the temperature of combustion flue gas) and therefore, the possible use of physisorbents in CO_2 will require cooling of the flue gas. In addition, most physical sorption technologies are not specifically selective towards CO_2 and must operate under dry conditions to avoid water competing for adsorption sites. This need to de-humidify the gas feed adds extra costs. Although hydrophobic sorbents have been developed to tackle the problem associated with selectivity towards water,[13,14] there remains a need to reduce the production cost of these complex synthetic sorbents. As an alternative, cryogenic separation technologies

Ocean Cheung is an assistant professor at the Division of Nanotechnology and Functional Materials at Uppsala University, Sweden. He holds a Master of Chemistry (MChem) degree from the University of Warwick, UK and a PhD in Materials Chemistry from Stockholm University, Sweden. His research is focused on the development of functional porous materials for environmental and bio-applications. Focused application areas within Dr Cheung's research include gas/vapour adsorption/separation, catalysis water treatment, and controlled drug delivery.

Wen Liu completed his training as a chemical engineer at the University of Cambridge. He is currently an Assistant Professor at the School of Chemical and Biomedical Engineering, Nanyang Technological University. Dr Liu's research focuses on studying carbon capture and utilisation (CCU) processes, from understanding the atomic scale reaction mechanisms, to designing new CCU strategies using process intensification strategies. He has a special interest in using hypothesis-driven methods to develop high performance oxide materials for carbon capture, oxygen transport, thermochemical water splitting and heterogeneous catalysis.

exploit the difference in the boiling points of the gas molecules, such that CO_2 can be extracted from the process gas mixtures *via* distillation or anti-sublimation.[15] Therefore, cryogenic separation is capable of producing CO_2 of very high purity that can be readily transported and utilised without further processing. However, the supply of cryogenic chill is often costly, both in terms of capital expenditure (CAPEX) and operational costs (OPEX), unless a low-cost cold energy source (*e.g.* the latent heat of the vaporisation of liquified nature gas) is available.[16]

Membrane technology offers process simplicity and scalability for extracting CO_2 from gas mixtures.[17] Unfortunately, the requirement for high pressure gradients across the membranes and the low durability of the membrane materials present notable technical challenges to the large-scale deployment of membrane-based for CO_2 capture technologies.[18]

In order to address the practical issues (*e.g.* thermal degradation and corrosiveness) associated with liquid amine scrubbing, the use of solid sorbents, such as solid amines and alkali metal oxides, has been proposed. In the latter case, the solid oxide sorbents occupy a large compositional space with versatile chemical formulations that can be tailored for a variety of CO_2 capture applications.[19] For example, the temperatures at which the sorbents take up and release CO_2 can be tuned by design. Different types of sorbents (*e.g.* physisorbents, liquid absorbents and high temperature solid sorbents) take up CO_2 *via* different mechanisms and have different operational conditions, it is therefore, not always possible to compare the different types of sorbents directly. Here, we review the recent developments of solid oxide sorbents, with a focus on synthetic strategies towards improved CO_2 capture performance.

1.2 Reversible CO_2 uptake by metal oxide sorbents

Metal oxides capable of chemically taking up CO_2 typically contain alkali metals and, or alkaline earth metals. The reversible capture of CO_2 by the metal oxide sorbents can be generalized by:

$$M_xO + CO_2 \rightleftharpoons M_xCO_3 \quad (1)$$

where $x = 1$ and 2 for alkaline earth metals and alkaline metals, respectively. The forward reaction involves carbonating the sorbent in flue gases with typical CO_2 mole fractions in the range of 3–20%. The carbonation takes place in the carbonator exothermically at a low temperature, at which the equilibrium CO_2 partial pressure is below 0.001 bar, such that almost all the CO_2 in the gas stream can be cleaned up by the sorbent. The reverse reaction (*i.e.* sorbent regeneration) involves decomposing the carbonate produced in virtually pure CO_2, such that the gaseous product is also a stream of pure CO_2, which can be further purified and compressed for storage and, or utilisation. The regeneration takes place endothermically at a high temperature, at which the equilibrium CO_2 partial pressure of the reaction system exceeds 1 bar, so all of the carbonated sorbent would irreversibly decompose. Plots of the equilibrium partial pressures of CO_2 for the carbonation of the binary oxides of alkali metals and alkaline earth metals are shown in Fig. 1a. Note that Fig. 1a excludes elements that are either deemed too expensive (*viz.* Rb_2O and CsO) or having considerable radioactivity (*viz.* Fr_2O and RaO). Based on the equilibrium temperatures for reversible CO_2 capture and regeneration, we define three types of solid oxide sorbents: (i) CaO, which reversibly takes up CO_2 at high temperatures, (ii) MgO, which reversibly takes up CO_2 at near-ambient temperatures, and (iii) all other oxides (Li_2O, Na_2O, K_2O, SrO and BaO), which are very strong bases whose carbonates require impractically high temperatures (*e.g.* above the melting point of the carbonates) to decompose. The ease to decompose the carbonates (as depicted in Fig. 1a) correlates well to the optical basicity of the binary

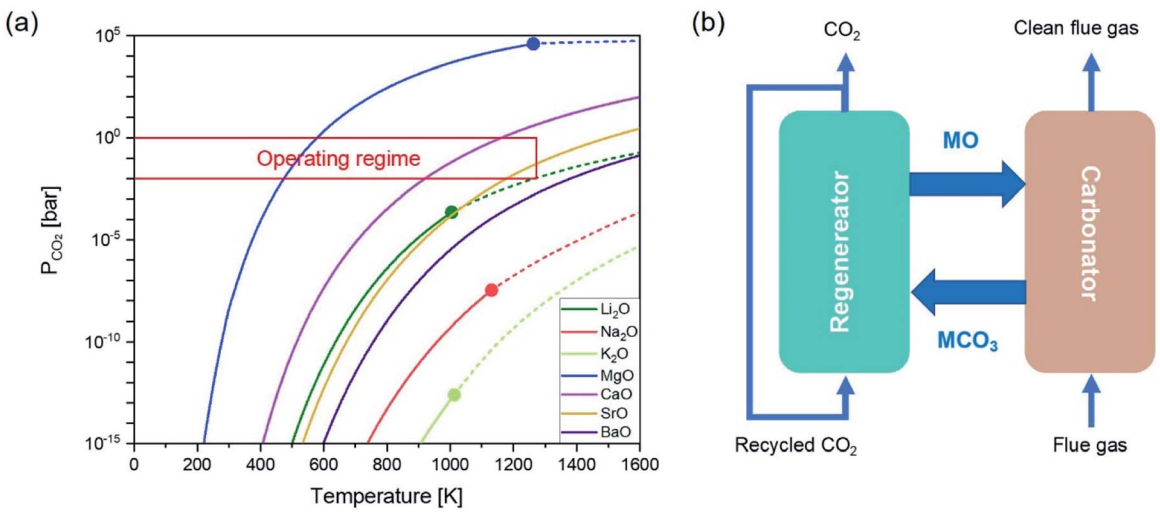

Fig. 1 (a) Equilibrium curves of partial pressures of CO_2 for the carbonation of the binary oxides of alkali metal/alkaline earth metal as functions of temperature. The red shaded area indicates CO_2 partial pressures that are practically achievable in a continuous CO_2 capture system. The discontinuities of the equilibrium curves changing from solid lines to dashed represents the melting point of the corresponding carbonates. (b) Schematic illustration of post-combustion CO_2 capture by solid sorbents in interconnected fluidised beds.

Table 1 Optical basicity of oxides based sorbents[23,24]

Cation	Oxide	Basicity
Mg^{2+}	MgO	0.78
Ca^{2+}	CaO	1.0
Li^{+}	Li_2O	1.0
Sr^{2+}	SrO	1.1
Ba^{2+}	BaO	1.15
Na^{+}	Na_2O	1.15
K^{+}	K_2O	1.4

metal oxides, as shown in Table 1, *i.e.* the carbonates derived from oxides with high optical basicity are generally hard to decompose during regeneration. Therefore, the basicity of type (iii) oxides are often chemically modified to enable reversible CO_2 uptake under practically accessible conditions.

As there is a temperature gap between the carbonation and the calcination steps, continuous CO_2 capture typically requires circulating the sorbents between two reactors, *viz.* a carbonator and a calciner. A common reactor configuration to achieve the swings between carbonation and regeneration is a set of interconnected fluidised beds, as depicted in Fig. 1b.[20–22]

Microscopically, the solid oxide sorbent particles undergo significant morphological changes as they cyclically take up and release CO_2. Although the carbonation of different types of sorbents follows different reaction mechanisms, there are some commonalities. During CO_2 capture, the sorbent typically develops a layer of carbonate, restricting the access of CO_2 to the unreacted oxides, thus reducing the overall rates of CO_2 uptake. In addition, the carbonates formed generally have low melting points, causing the sorbents to sinter, thereby hindering their performance in subsequent capture cycles. Because of these limitations, there are considerable gaps between the sorbents' stoichiometric CO_2 uptake capacities and those practically accessible after multiple carbon capture cycles. To improve the overall efficiency and effectiveness of the oxide-based CO_2 capture processes, a significant amount of research is required to understand the sorbent behaviour and subsequently to rationally design high performance sorbents, often by optimising the synthesis approach. In general, an ideal solid oxide sorbent should (i) be able to undergo reversible carbonation at temperatures that are closely matching the temperatures of the upstream/downstream processes, (ii) have fast uptake and release kinetics, (iii) exhibit stable performance over large number of CO_2 capture cycles, (iv) have sufficient physical hardness to survive prolonged attrition in circulating fluidised beds and (v) can be produced in large quantities with relatively simple methods and low costs.

1.3 Objective and review outline

Over the past decades, there have been large number of studies that develop and investigate solid oxide CO_2 sorbents, with focuses on both the process and materials aspects. The interested reader is referred to past reviews which provide broad overviews of CO_2 capture technologies employing solid sorbents,[25] and in particular metal oxide-based solid sorbents.[26] It is worth noting that the studies addressing the materials challenge ubiquitously point towards the need to develop high-performance synthetic sorbents. Despite the abundant reports of synthetic sorbents showing improvements over natural sorbents such as limestone, the relationships between the sorbents' compositions, synthesis methods, structures and CO_2 capture behaviour are still not fully understood. Therefore, given the rapid development in characterisation techniques and synthesis methods, we see the need for a critical assessment of the literature focusing the recent advances in synthetic strategies for preparing high performance metal oxide based CO_2 sorbents with the following specific objectives:

- Review the state-of-the-art understanding of the behaviour of the oxide sorbents over CO_2 capture cycles.
- Review different synthetic approaches for preparing high performance oxide sorbents.
- Identify knowledge gaps in understanding the behaviour of synthetic sorbents under realistic CO_2 capture conditions.
- Highlight emerging approaches for improving the performance of synthetic sorbents.
- Promote the need for standards for evaluating the performance of newly developed CO_2 sorbents.

2 CaO based sorbents

CaO based sorbents are the most commonly discussed due to their high CO_2 uptake capacity, fast carbonation and regeneration rates, high earth-abundance and low cost. In Table 2 we summarise the CO_2 uptake properties of a number of recently reported CaO based CO_2 sorbents. The reversible reaction between CaO and CO_2 is also known as calcium looping or calcium carbonate looping:

$$CaO(s) + CO_2(g) \rightleftharpoons CaCO_3(s),\ \Delta H_{298} = -178\ kJ\ mol^{-1} \quad (2)$$

The forward reaction typically takes place around 650 °C, whereas regeneration takes place in 1 bar CO_2 at >900 °C.[4] The CaO sorbents can be applied to both pre- and post-combustion CO_2 capture at power stations, as well as CO_2 capture from industrial processes such as cement production.[27,28] In the case of pre-combustion capture,[29] CaO facilitates the sorbent-enhanced water gas shift to produce highly concentrated H_2:[30]

$$CaO(s) + H_2O(g) + CO(g) \rightleftharpoons CaCO_3(s) + H_2(g) \quad (3)$$

In addition, CaO based sorbents can be used for capturing CO_2 produced by cement plants.[31] In fact, CaO based capture process can be efficiently integrated into the cement production process,[32] requiring only minor modifications to the existing equipment and process, whilst reducing the fuel consumption and CO_2 emissions by ~75% and ~85%, respectively.[33] Because of the relative ease to prepare CaO based sorbents at large batches, the integration of CaO based carbon capture has been demonstrated at pilot scales (to up 1.9 MWth) by various research groups.[34,35] Freshly prepared CaO sorbents, without any further modification, could easily take up CO_2 close to the

Table 2 Various reaction conditions and capacities of CaO based sorbents[a]

Sorbent					Conditions						Capacity			
											CO_2 uptake		Cycle capacity	
Name of the sorbent	Base (B)	Support (S)	Fraction of S	Method	Carbonation temperature [°C]	Calcination temperature [°C]	Carbonation time [min]	Calcination time [min]	CO_2 [%]	BET [m^2 g^{-1}]	[wt%]	[mol%]	[loss%/χ cycle]	Ref.
S20-4x	$Ca(NO_3)_2 \cdot 4H_2O$	$Zr(NO_3)_2 \cdot 6H_2O$	0.1	e	675	850	20	10	20	12	41.8	53.3	0.8/20	53
S20-6x	$Ca(NO_3)_2 \cdot 4H_2O$	$Zr(NO_3)_2 \cdot 6H_2O$	0.1	e	675	850	20	10	20	20	49.7	63.4	7.3/20	53
S20-8x	$Ca(NO_3)_2 \cdot 4H_2O$	$Zr(NO_3)_2 \cdot 6H_2O$	0.1	g	675	850	20	10	20	23	48.9	62.2	5.7/50	53
CL-CE-75	Calcium L-lactate hydrate	$CaO \cdot Al_2O_3$ cement	0.25	f	650	900	30	10	15	—	36	45.9	—/70	74
CC-AN-80														
$Ca_3(C_6H_5O_7)_2 \cdot 4H_2O$	$Al(NO_3)_3$	0.2	b	650	800	30	10	15	10	59	75.2	14/28	75	
CaO-SBA15	$Ca(CH_3COO)_2$	SBA	0.5	b	700	910	60	30	100	155	43.1	55	20/40	76
CaO-CC	$CaCO_3$	—	—	—	650	120	950	30	15	1	71.2	90.7	23.75/11	77
CaO-ES	$CaCO_3$	$MgCO_3$	—	—	650	120	950	30	15	1	61.8	78.8	20.41/11	77
CaO–P	$CaCl_2$	—	—	c	650	120	950	30	15	5	48.6	61.9	2.97/11	77
Ca–Al–CO_3	CaO	Al_2O_3	0.5	c	600	700	45	20	50	—	55.7	71	—/10	66
Ca–Al–CO_3	CaO	Al_2O_3	0.5	c	600	700	25	20	50	—	56.7	72.3	—/30	66
$Ca_1Ni_{0.1}$	$Ca(NO_3) \cdot 4H_2O$	$Ni(NO_3)_2 \cdot 6H_2O$	0.1	d	650	650	25	3	15	13	66.0	84.1	—/20	55
$Ca_1Ni_{0.1}Ce_{0.033}$	$Ca(NO_3) \cdot 4H_2O$	$Ce(NO_3)_2 \cdot 6H_2O$	0.033	d	650	650	25	3	15	21	62.1	79.1	—/20	55
CNAN-SG	$Ca(NO_3)$	$Al(NO_3)_3 \cdot 9H_2O$	0.3	d	650	900	5	5	15	13	27.5	35	28/21	65
CAAN-SG	$Ca(CH_3COO)_2$	$Al(NO_3)_3 \cdot 9H_2O$	0.3	d	650	900	5	5	15	12	13.6	17.3	40/21	65
CaO-GS 2 mM	CaO	Gemini surfactant	0.0008	f	600	850	—	30	15	16	29.0	37	—	72
CaO-SDS 20 mM	CaO	Sodium dodecyl sulfate	0.008	f	600	850	—	30	15	9	27.0	34.4	—	72
CaO-(s-s)	CaO	ZrO_2	0.03	e	650	780	120	60	Pure	—	57.7	73.5	—	58
CaO-(c-sg)	CaO	ZrO_2	0.03	d	650	780	120	60	Pure	—	77.5	98.7	—	58
$CaO/CaZrO_3$	$Ca(NO_3)_2 \cdot 4H_2O$	$ZrO(NO_3)_2 \cdot xH_2O$	0.14	d	650	850	30	5	15	—	~48.0	61.1	7/50	68
CaO–ZrO_2–SG	CaO	ZrO_2	0.1	d	200	900	—	—	—	25	65.0	82.8	—/20	59
CaO–ZrO_2–IM	CaO	ZrO_2	0.1	b	200	900	—	—	—	19	64.0	81.6	6.25/14–20	59
Ca-hyd_95:5_2 h	$Ca(OH)_2$	ZrO_2	0.05	d	800	800	5	15	50	12	51.0	65	39.22/90	78
Ca-hyd_95:10_2 h	$Ca(OH)_2$	ZrO_2	0.1	d	750	750	20	10	40	11	52.0	66.3	5.77/10	78
C74D26	Carbide	Dolomite	0.35	a	700	850	20	10	15	14	54.0	68.9	—/10	79
Mg/Ca-0.2	$Ca(CH_3COO)_2$	$Mg(NO_3)_2$	11	d	700	700	30	30	Pure	—	59.2	75.4	4.7/7	80
Ca/Al-2.5–1%	CaO	Al_2O_3	0.4	c	600	700	45	20	100	6	59.1	75.3	5.9/220	48
Ca-CNT	CaO nanotube	—	—	—	650	850	30	10	15	12	58.0	73.9	34.48/15	81

[a] (a) Combustion, (b) impregnation, (c) precipitation, (d) sol–gel, (e) solid-state, (f) wet-mixing, (g) solution-combustion.

stoichiometric capacity of 78 wt% (based on the mass of the fully calcined CaO)[36,37] however, the performance of unmodified CaO sorbents will rapidly deteriorate over uptake–regeneration cycles as a result of sintering,[38,39] as the surface area and accessible pore volumes of the sorbents rapidly diminish. In continuous operation, the deactivated sorbents act as inert materials, which imposes significant energy penalty as they participate in the temperature swing cycles without capturing CO_2. The deactivation mechanism during calcium looping cycles has been extensively studied.[32,40–42] The biggest challenge of using CaO sorbents is to develop solutions that address their poor cyclic stability. The two general strategies to improve the performance of calcium looping systems are (i) optimising operating conditions and (ii) prepare high performance synthetic sorbents, as discussed in the following sections.

2.1 Optimising operating conditions

The performance of the CaO based sorbents depends on the operating conditions. Accordingly, researchers have exploited such dependence to delay or mitigate sorbent deactivation over calcium looping cycles. For example, the presence of steam in the calcium looping reactors is found to influence both reaction rates and mass transfer[43,44] specifically, steam is known to enhance the rate of calcination.[45,46] In addition, experimental observations suggest that operation in the presence of steam increases the porosity of the sorbents, and subsequently improve their CO_2 capture performance in terms of both reaction kinetics and cyclic stability.[47,48]

The issue of sorbent deactivation can also be circumvented by reactivating the spent sorbents. The recent study by Sun *et al.*[49] provided insights into the effects of different reactivation methods on the cyclic performance of CaO/MgO (CaO : MgO mass ratio = 75 : 25) sorbents, obtained using calcium acetate monohydrate and magnesium acetate tetrahydrate as precursors. Sun *et al.*[49] tested different sorbent reactivation methods: (i) hydration, (ii) hydration/impregnation and (iii) acidification. Good cyclic stability was observed when the sorbent was reactivated by hydration or hydration/impregnation, rendering CO_2 uptake of 39 and 41.4 wt% (49.7 and 52.8 mol%) after 40 cycles, respectively. In both cases, the CO_2 uptake increase with the number of cycles due to "self-activation". Self-reactivation, sometimes referred to as "deep carbonation", is a phenomenon that can be explained using the pore skeleton model by Manovic and Anthony,[50] as depicted in Fig. 2. An inward hard skeleton is formed during calcination. However, the hard skeleton hampers the ion diffusion through the product layer of $CaCO_3$, impeding the rate of carbonation during the initial cyclic operation. Over the carbonation–regeneration cycles, the soft skeleton is gradually activated and contributes to an increase rate of carbonation.[50]

Sorbent reactivation by acidification is relevant for removing the irreversibly formed $CaSO_4$ due to the presence of SO_2 in the flue gas. For a CaO : MgO sorbent, reactivation by acidification resulted in a CO_2 uptake of 23.3 wt% (29.7 mol%) after 40 cycles. Thus, acidification as a reactivation method needs further development to overcome the high cost and the potential release of toxic substances.[49]

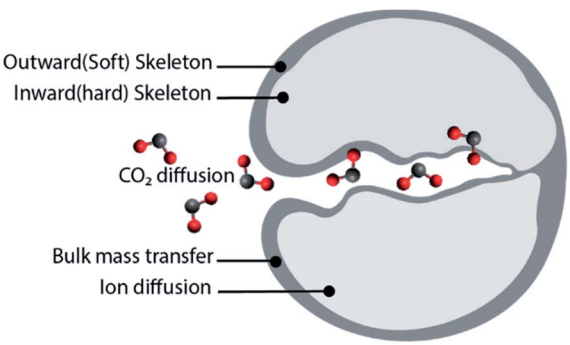

Fig. 2 The pore skeleton model for CO_2 and ion diffusion. Illustrated according to the finding presented in ref. 51.

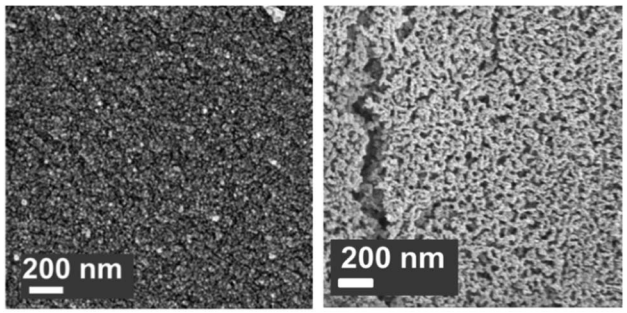

Fig. 3 Scanning electron micrograph of CaO stabilised with both MgO and Al_2O_3 (left) as-synthesised and (right) after 23 cycles of carbonation/calcination.[56]

2.2 Synthetic CaO based sorbents stabilised by inert supports

In addition to employing reactivation steps, the cyclic performance of CaO sorbents can be fundamentally improved by mixing CaO with inert refractory materials (*e.g.* Al_2O_3, ZrO_2,

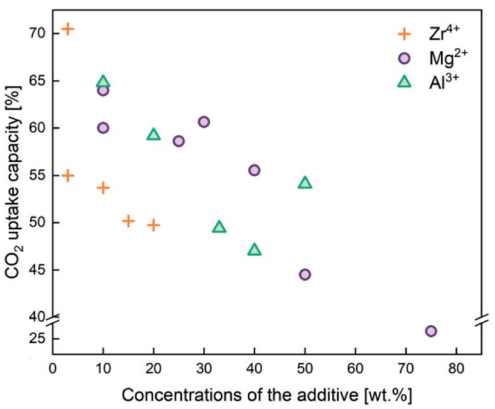

Fig. 4 CO_2 capture capacity of CaO based sorbents stabilised by the three different typical sintering-resistant, oxidic additives containing Zr^{4+}, Al^{3+}, and Mg^{2+}. The effect of these additives on the cyclic stability of CaO sorbents is summarised in Table 2.

MgO and their derivatives) to render additional sintering resistance and physical hardness. A number of studies have reported CaO based sorbents supported on varying amounts of refractory materials. The resulting CO_2 uptake capacity also varied, partly due to the differences in the overall compositions, as shown in Fig. 4. The stabilising effects of adding different types and amounts of thermally stabilising cations, referencing notable recent works, are summarised in Table 2 and discussed below.

Soleimanisalim *et al.*[52] used $CaCl_2 \cdot 2H_2O$ and a small amount of $ZrO(NO_3)_2 \cdot 6H_2O$ as precursors to prepare a stabilised CaO sorbent containing 10 wt% $CaZrO_3$ perovskite by the solution combustion method. The resulting CaO sorbent showed a high CO_2 uptake of ~53.3 wt% (68.2 mol%) in the first cycle and ~42.7 wt% (54.41 mol%) after 31 cycles. The stabilising effect of $CaZrO_3$ was also reported by Hashemi *et al.*[53] who found 20 wt% $CaZrO_3$ to be optimal for maintaining cyclic stability (46.2 wt% (58.87 mol%) after 20 cycles). To maximise cyclic stability and CO_2 capture performance, the type of stabiliser and the amount of stabiliser were optimized in the relevant studies.[43,44] Specifically, Guo *et al.*[39] showed that the Ca : Al ratio of Ca–Al mixed oxides ($Ca^{2+}/Al^{3+} = 2, 2.5, 3, 3.5, 4$) synthesised by coprecipitation affected the CO_2 uptake capacity. The Ca : Al ratio of 2.5 gave the highest CO_2 uptake capacity of around 47 wt% (60 mol%) after 3 cycles. The high CO_2 capacity and reasonable cyclic performance was attributed to the large pore size and the small particle size. Compared to the morphological properties, the amount of $Ca_{12}Al_{14}O_{33}$ present was also found to be a crucial factor in determining the sorbent's CO_2 capture capacity.[48,52,54] Sun *et al.*[55] revealed that CeO_2 can be used as an effective physical barrier to prevent the sintering of CaO. Similarly, Vall *et al.*[56] employed MgO and Al_2O_3 to stabilise a synthetic CaO sorbent, obtained by calcining highly porous amorphous calcium carbonate (HPACC–BET surface area of over 450 $m^2\ g^{-1}$). Whilst MgO alone can effectively stabilise the CaO sorbent, the sorbent synergistically stabilised by both MgO and Al_2O_3 yielded even higher stability, showing only a 2.8% decrease in the CO_2 uptake capacity after 23 cycles (1st cycle 54.2 wt%, 69.1 mol%). Scanning electron micrographs (SEM) (Fig. 3) of the CaO stabilised with both MgO and Al_2O_3 confirmed the effective hinderance of sintering after 23 cycles.

2.2.1 Preparing supported sorbents by sol–gel method. The effective mixing between CaO and thermal stabilisers (*i.e.* support materials) is critical to enhancing the cyclic CO_2 capture performance. Conventional preparation methods, such as mechanical mixing, impregnation and co-precipitation may not provide sufficient dispersion of the thermal stabilisers within the sorbent matrix. To this end, sol–gel method has been explored as an alternative strategy to prepare supported CaO sorbents.[57] In general, sol–gel methods can induce and control the chemical interaction between the inert supports and CaO, whilst allowing the facile control of particle size and surface area. Yoon *et al.*,[58] Sultana *et al.*[59] and Gao *et al.*[60] all showed that CaO based sorbents prepared by sol–gel synthesis result in increased specific surface areas and pore volumes. The increased porosity can come from reduced particle size, leading to shortened CO_2 diffusion paths and consequently accelerated rate of CO_2 capture. For example, Zr-modified CaO prepared by Yoon *et al.*[58] had small particle sizes of ≤2 μm, high CO_2 uptake of 73.2 wt% (93.3 mol%) (compared to 54 wt% (69 mol%) of the sorbent prepared by physical mixing). In addition the CO_2 uptake capacity sustained at ~70.5 wt% (89.8 mol%) over 10 cycles.[58] Sultana *et al.*[59] prepared nano-CaO coated with ZrO_2 by sol–gel, wet impregnation, and hydrolysis methods. They found that sol–gel synthesis gave the most stable $CaZrO_3$ protective layer on the surface of the nano-CaO, with excellent CO_2 uptake of 65 wt% (83 mol%) after 20 cycles, as shown in Fig. 5.[59] Similarly, Gao *et al.*[60] synthesised CaO supported on charcoal by physical mixing, sol–gel, and wet impregnation and found that the CaO supported on charcoal by sol–gel method showed a high CO_2 capture capacity of 66.5 wt% (84.7 mol%).[60] In both studies, the sol–gel methods produced sorbents with the higher pore volumes, surface areas, CO_2 uptake and cyclic stability than sorbents prepared by other methods.

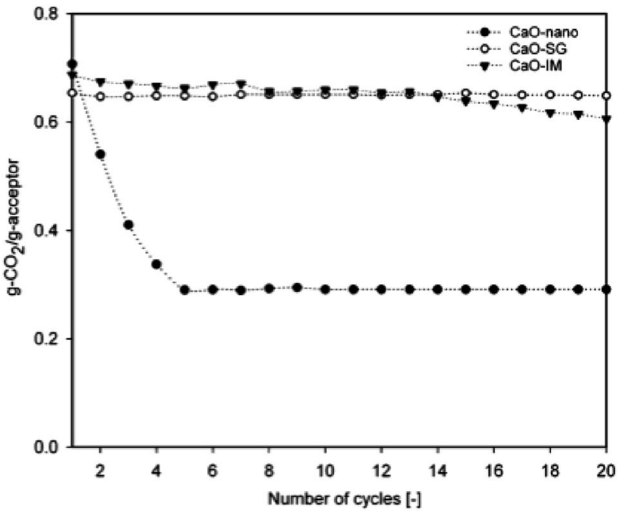

Fig. 5 CO_2 capture capacity of nano-CaO by sol–gel and wet impregnation methods. Reprinted with permission from ref. 59. Copyright 2021 American Chemical Society.

2.2.2 Core–shell structured sorbents. One special type of stabilised CaO based sorbents is core–shell structured sorbents, where the stabilising oxides form shells encapsulating the CaO cores. In effect, the inert shells form continuous physical barriers, preventing the cores from fusing into each other. Han *et al.*[61] synthesised the CaO@Al_2O_3 core–shell structure sorbent and observed 41 wt% (52 mol%) of CO_2 uptake after 20 cycle with Al_2O_3 shell thicknesses of between 4 to 8 nm. The covered cores (CaO) have resisted sintering over CO_2 capture cycles.[61] The thickness of the shell can be one of the factors determining the overall CO_2 capture performance. Armutlulu *et al.*[62] prepared CaO@Al_2O_3 core–shell sorbents, with three different shell thicknesses. The thickness around 2.75 nm reported relatively good stability and CO_2 uptake capacity of ~55 wt% (70 mol%) after 30 cycles, whereas thicker Al_2O_3 layers lead to lower initial CO_2 uptake.[62] In addition to the CaO@Al_2O_3 design, Peng *et al.*[63] added TiO_2 as a secondary stabiliser. The resulting CaO@TiO_2–Al_2O_3 showed high stability and CO_2

uptake of 46 wt% (59 mol%) after 104 cycles.[63] Using a 2.7 nm Al_2O_3 coating on CaO nanoparticles, Kurlov *et al.*[54] demonstrated a 140% improvement in CO_2 uptake over a limestone reference and excellent cyclic stability (41 wt% (52 mol%) uptake after 10 cycles). They found the addition of the Al_2O_3 layers induced the formation of inert $Ca_{12}Al_{14}O_{33}$ and $Ca_3Al_2O_6$ on the surface of CaO nanoparticles, produced by the calcination of calcite obtained by sacrificial template synthesis, with an average particle size of 350 nm and a BET surface area of 16 m^2 g^{-1}. Consequently, the shell layer consisting of $Ca_{12}Al_{14}O_{33}$ and $Ca_3Al_2O_6$ acts as an effective thermal stabiliser.[54]

2.2.3 Effect of synthesis parameters. It is well established that the CO_2 uptake performance, including kinetics and cyclic stability, are functions of the sorbents' starting structures, which are in turn determined by the synthesis parameters used during sorbent preparation. For early literature on the synthesis of CaO based sorbents, we refer the reader to the reviews by Liu *et al.*[64] and Kierzkowska *et al.*[29] Here, we focus on recent studies (last ~5 years) investigating the effects of key synthesis parameters, as discussed in the following.

Precursors. Although the exact roles and effects of the various chemical precursors may differ, they are nonetheless critical to the performance of the synthesised sorbents. Azimi *et al.*[65] demonstrated that different combinations of Ca and Al precursors yield sorbents with noticeably different particle sizes, surface areas and morphologies. For instance, for the sol–gel synthesis of a CaO based sorbent, highly soluble nitrate precursors such as calcium nitrate (CN) and aluminium nitrate (AN) form inert phases such as $Ca_{12}Al_{14}O_{33}$ and $Ca_9Al_6O_{18}$ more easily than the nitrate-free precursors. The insoluble precursors such as nano-structured alumina (nA) formed a more compact structure than the ones prepared from aluminium nitrate (AN), which yielded a "fluffy structure" with a surface area of 13 m^2 g^{-1} and a mean particle size ~16.9 nm. Overall, the Al-supported CaO sorbent synthesised with soluble nitrate precursors showed the highest CO_2 uptake (91.7 wt% (117 mol%), with 28 wt% loss after 21 cycles) than sorbents synthesised from other types of precursors.

Synthesis and calcination temperatures. Temperature is a factor that can be used to control the surface area and particle size of CaO based sorbents. Kou *et al.*[66] observed that high synthesis temperature promoted crystal growth and particle aggregation in Ca–Al mixed oxides. The average particle size of the samples also increased from 29.5 nm for the synthesised at RT to 42.1 nm for the sorbent synthesised at 80 °C. In fact, the crystallinities of CaO, Ca–Al spinel and $CaCO_3$ all increased with increasing synthesis temperature, as shown in Fig. 6. On the other hand, the increase in particle size is accompanied by a decrease in CO_2 capture capacity.

Apart from the temperature of the wet-synthesis, the calcination temperatures also affect the surface areas and pore volumes of the sorbents. Wang *et al.*[67] observed during the synthesis of $CaO/CaZrO_3$ hollow spheres that the heating rate of calcination significantly affected the cyclic stability of the sorbent – a slow heating rate of 5 °C min^{-1} resulted in a stable (capacity decreased by <5 wt% after 30 cycles) compared to a sorbent prepred with a calcination rate of 20 °C min^{-1}

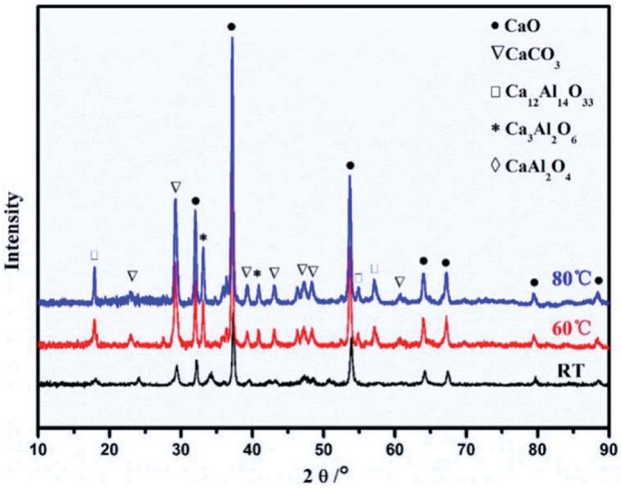

Fig. 6 XRD patterns of the Ca–Al mixed oxides (Ca^{2+}/Al^{3+} = 3) synthesised at room temperature (RT), 60 °C and 80 °C. Reprinted with permission[66] copyright 2021 Elsevier.

(capacity decreased by <20 wt%).[67] Antzara *et al.*[68] performed the calcination of ZrO_2 promoted CaO at 750 and 800 °C and found that low calcination temperature (750 °C) reduced sintering during carbonation and resulted in CaO with high surface area and pore volume compared to CaO/ZrO_2 sorbents calcined at 800 °C.[68]

Template. The templated synthesis of CaO based sorbent has been adopted for morphology control and to introduce macro porosity to the sorbent. Carbon based template is one of the most commonly used for the synthesis of structured CaO sorbents. Ping *et al.*[69] found that the cage-like $CaCO_3$ hollow spheres synthesised using $Ca(NO_3)_2$, urea and polysaccharide spheres template showed an excellent CO_2 uptake of up to 78.6 wt% (100.2 mol%) in the first cycle, 45 wt% higher than the same composition synthesised without the template. Colloidal carbon spheres derived from glucose were used as the template for the synthesis of $CaO/CaZrO_3$ and CaO sorbents.[67,70] Wang *et al.*[67] found that $CaO/CaZrO_3$ hollow spheres synthesised with $Ca(NO_3)_2$ and $Zr(NO_3)_4$, templated with carbon sphere (from glucose) had improved cyclic stability over 100 cycles. In a similar study, Wang *et al.*[70] prepared CaO based meshed hollow spheres by urea hydrolysis with carbon sphere (from glucose) template and demonstrated a high CO_2 capacity of ~75 wt% (96 mol%) in the first cycle, with a moderate capacity decrease of 12 wt% over 28 cycles. The authors suggested that the hollow sphere structures could produce porous CaO particles with improved CO_2 uptake.[70] In other similar studies, Naeem *et al.*[71] incorporated a carbon template, prepared by poly-condensation of resorcinol with an aqueous formaldehyde solution, to the sol–gel synthesis of a Al_2O_3 and Y_2O_3 supported CaO sorbent. The resulting structure consisting of interconnected microspheres of supported CaO had an uptake of CO_2 of 61 wt% (78 mol%), which remained unchanged after 10 cycles.[71]

Surfactants. Previous studies have shown the use of surfactant to be an effective way to control the particle size of CaO based sorbents. In a number of cases, such as Jamrunroj *et al.*[72]

Table 3 Various reaction conditions and capacities of MgO based sorbents[a]

Sorbent					Conditions						Capacity			
											CO_2 uptake		Cycle stability	
Name of the sorbent	Base (B)	Promotor (P)	Fraction of S	Method	Carbonation temperature [°C]	Calcination temperature [°C]	Carbonation time [min]	Calcination time [min]	CO_2 [%]	BET [$m^2\ g^{-1}$]	[wt%]	[mol%]	[loss%/cycle]	Ref.
MgO-AMS_{10}-325 °C	MgO	$LiNO_3$, KNO_3, Na_2CO_3, K_2CO_3	0.44, 0.56, 0.5, 0.5	c	325	450	180	90	HP	—	83.9	76.8	17/30	88
MgO-AMS_{10}-350 °C					350	450	240	60	HP	—	81.5	74.6	—	88
MgO–$NaNO_3$ + $NaNO_2$	MgO	$NaNO_3$, $NaNO_2$	0.07, 0.15	c	350	400	30	20	Pure	23	55.0	50.4	55.2/15	84
MgO–$NaNO_3$	MgO	$NaNO_3$	0.07	c	325	400	30	20	Pure	29	83.2	76.2	54.5/15	84
MgO–K_2CO_3	$Mg(NO_3)_2 \cdot 6H_2O$	K_2CO_3	3	b	375	400	20	30	100	2	8.6	7.8	5.1/17	104
MgO–KNO_3	MgO	KNO_3	0.2	c	325	450	20	30	100	107	10.2	9.4	2412	105
MgO–KNO_3	MgO	KNO_3	0.2	c	375	450	20	30	100	107	8.3	7.6	10/12	105
Na–Mg double salt	MgO	Na_2CO_3	0.1	a	375	500	—	—	Pure	—	15.4	14.1	0/7	106
MgO–Na_2CO_3	$Mg(NO_3)_2 \cdot 6H_2O$	Na_2CO_3	0.5	b	380	470	60	10	100	—	15.0	13.7	—/9	107
MgONaNa-0.1	MgO	Na_2CO_3, $NaNO_3$	0.1	b	325	450	60	10	Pure	39	45.2	41.4	34.96/14	91
1.00$NaNO_3$/MgO	MgO	$NaNO_3$	1	b	330	400	—	—	100	—	23.3	21.4	—/15	108
MgO–(Li/Na/K)NO_3	MgO	$LiNO_3$, $NaNO_2$, KNO_2	0.1	b	300	450	240	60	HP	19	73.9	67.7	—	109
MgO–(Li/Na/K)NO_3	MgO		0.1	b	350	350	30	30	HP	19	14.1	12.9	—/20	109
MgO–(Li/Na/K)NO_3	MgO		0.1	b	340	450	240	60	100	—	69.1	63.3	14/20	86
Mg_3Al_1–CO_3pH12	$Mg(NO_3)_2 \cdot 6H_2O$	$Al(NO_3)_3 \cdot 9H_2O$	0.3	c	200	400	—	60	—	—	3.7	3.3	—	110
$NaNO_3$-5Mg30-MgO	$Mg(NO_3)_2 \cdot 6H_2O$	$NaNO_3$	0.2	d	300	450	180	60	100	—	11.5	10.5	+19.02/8	111
MgO$NaNO_3$	Hydrotalcite	$NaNO_3$	0.2	d	300	450	180	60	100	—	37.4	34.3	53.6/8	111
MgO-10%CeO_2	MgO–CeO_2	$LiNO_3$, KNO_3, Na_2CO_3, K_2CO_3	0.17	a	325	425	60	15	100	252	35	32.1	+1.22/30	112
5A5M	$Mg(NO_3)_2 \cdot 6H_2O$	$Al(NO_3)_3 \cdot 9H_2O$	1	a	200	600	60	60	10	177	13.1	12	12/6	113
MgO-AC	$Mg(NO_3)_2 \cdot 6H_2O$	NH_4OH	5	c	300	400	60	—	UP	362	5.2	4.7	42/27	96

[a] (a) Sol–gel, (b) wet mixing, (c) precipitation, (d) physical mixing, (HP) high purity, (UP) ultra purity.

and Chen *et al.*,[73] there is an optimal amount of surfactant that is required to produce high performance sorbents. Jamrunroj *et al.*[72] found that 2 mM of gemini (GS: 12-carbon hydrophobic chains and 3 carbon alkyl spacer, 12–3–12) yielded the best CO_2 capture performance. The resulting CaO–GS-2 mM sorbent, having small particles of (~37 nm) and high surface area (16 $m^2 g^{-1}$), showed the highest CO_2 uptake (29 wt% (37 mol%)) amongst all the CaO–GS sorbents tested.[72] Similarly, Chen *et al.*[73] concluded that the best performing CuO/CaO sorbent was obtained with a low H_2O : cetyltrimethyl ammonium bromide ($C_{19}H_{42}BrN$, CTAB) molar ratio of 23 : 1. This low CTAB ratio is important for producing small particles (46.5 nm) with a CO_2 uptake of 13 wt% (17 mol%), which decreased to 10 wt% (13 mol%) after 19 cycles.[73] These studies exemplify that optimal levels of surfactant are crucial for producing sorbent materials with small particle sizes and high capture performance. However, in the case of CaO synthesised with sulphonic single chain (SDS), 40 mM of SDS yield the smallest particles with the lowest CO_2 uptake of 18 wt% (23 mol%) compared to other SDS doping amount.[72] Therefore, the surfactant effect cannot be easily generalised. In addition, factors such as the micellar structures and the interfacial adsorption ability of the surfactant should also be thoroughly understood and carefully considered during synthesis.

2.3 Summary and knowledge gap

CaO based CO_2 sorbents are promising for capturing CO_2 at high temperatures. These sorbents show high CO_2 uptake capacities with rapid uptake kinetics. Significant advances have been made to improve the performance of the sorbents through carefully tuned synthetic procedures and formulations. However, major challenges remain for the efficient, robust, long term, cost-effective application of CaO based sorbents. Besides steam injection and sorbent reactivation, there are a number of synthetic approaches to enhance the uptake and cyclic stability of CaO sorbents, primarily involving supporting CaO with thermally stable support materials and optimising synthetic parameters. Challenges lie in gaining an in-depth understanding of the effectiveness of each approach, and how they can be synergistically combined to enhance the performance of the CaO sorbents. On that front, we find the use of surfactant in the synthesis of CaO sorbents a particularly interesting avenue for further research. Making good use of surfactants' surface chemistry could hold the key to producing stable, small and porous CaO particles.

3 MgO based sorbents

Magnesium oxide (MgO) captures CO_2 by:

$$MgO(s) + CO_2(g) \rightleftharpoons MgCO_3(s); \Delta H_{298} = -118 \text{ kJ mol}^{-1} \quad (4)$$

The reversible CO_2 capture can be carried out over the temperature range between 200 and 400 °C, making it suitable for heat integration with processes where abundant low-grade heat is available. Although the maximum theoretical CO_2 uptake by MgO sorbent is high (110 wt%, 101 mol%), the practically accessible uptake capacity is no more than 10 wt%, owing to the formation of an impermeable layer of $MgCO_3$, which effectively stops the encapsulated MgO from further carbonation. On the other hand, the low operating temperatures could mitigate sorbent deactivation by sintering. Therefore, the majority of the research efforts in developing synthetic MgO based sorbents focus on improving the CO_2 uptake capacities through physical and chemical modifications, including (i) introducing dopants to promote the reaction with CO_2 or (ii) preparing nanostructured MgO with very large specific surface areas to minimise the encapsulation of MgO by $MgCO_3$. A recent review by Hu *et al.*[82] focuses on the development of MgO sorbent for CO_2 capture and provides a detailed insight in this topic. Here, we present a focused discussion on the synthesis and performance of these MgO sorbents. A list of recently developed MgO sorbents and their CO_2 capture performance is shown in Table 3, with key papers discussed in the following sections.

3.1 Promoted MgO sorbents

Recently, the used of alkali metal nitrates has been in the spotlight as a means to improve CO_2 capture performance of MgO based sorbents. The use of alkali metal nitrates exploits the fact that they melt during the CO_2 capture process. The molten nitrate prevents the formation a solid $MgCO_3$ layer on the surface of MgO. Fig. 7 illustrates the function of the molten nitrate to promote the carbonation of MgO. The most commonly used nitrate promoters are $NaNO_3$ and KNO_3. Because these nitrates do not directly react with CO_2, the CO_2

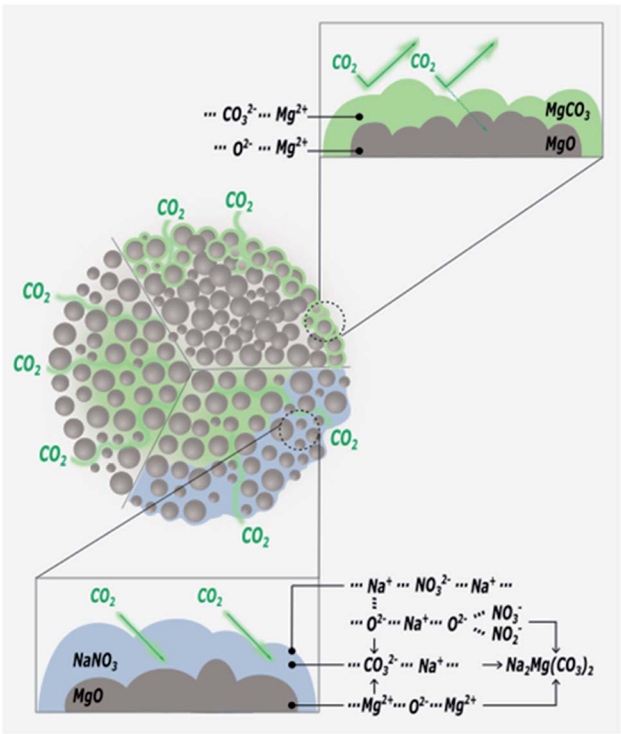

Fig. 7 The role of the MgO sorbent with nitrate salts for improving CO_2 capture capacity.

capture capacity is governed by the amount of active MgO available in the solid.[83] In addition to alkali metal nitrates, alkali metal carbonates could also enhance the performance of MgO sorbents, rendering both faster kinetics and higher uptake capacity. Further enhancements can be achieved when carbonate and nitrate promoters are used concomitantly. These different approaches to promote MgO sorbents are discussed below.

3.1.1 Sodium nitrate ($NaNO_3$). The simple use of $NaNO_3$ as a promoter for MgO sorbent has been explored by a number of researchers. Studies using $NaNO_3$ as the only promoter have demonstrated effective promotional effects, reporting that doping ~7–11 mol% $NaNO_3$ by impregnation is the most effective in enhancing CO_2 uptake by MgO, despite the variabilities in CO_2 uptake report by different studies; the variabilities are likely to be results of the different synthesis procedures used.[52,84,85] Zhao *et al.*[84] studied calcined mesoporous MgO, synthesised by hydrothermal process (using $Mg(CH_3COO)_2$ and urea), and reported the highest CO_2 uptake of 66.90 wt% (61.3 mol%) on MgO promoted with 7 mol% of $NaNO_3$; this is over 40 times the CO_2 uptake by pure MgO 1.28 wt% (1.2 mol%). The promotional effect was associated with the formation of triple phase boundaries between the MgO, the promoters and the gas phase.[84] With too little $NaNO_3$, the reaction at the phase boundaries and at the outer layer of the carbonate would be limited. In contrast, too much $NaNO_3$ would reduce the solubility of CO_2 as well as the contact between MgO and CO_2, thus limiting the CO_2 capture capacity.[84]

3.1.2 Mixed metal nitrates. Mixed metal nitrates can also be used to create analogous promotional effects. Harada *et al.*[86] showed that 15 mol% (Li–Na–K)NO_3 on colloidal MgO nanoclusters prepared by sol–gel exhibited a high CO_2 uptake capacity of 69.10 wt% (63.3 mol%) at 340 °C. Dal Pozzo *et al.*[85] obtained promoted MgO by wet mixing commercial $MgCO_3$ with metal salts, followed by calcination at 450 °C. They showed that (Li, Na)NO_3, (Li, K)NO_3 and (Li, Na, K)NO_3 all promoted MgO sorbents in a similar manner to when $NaNO_3$ was the only promoter, reporting CO_2 uptake ~38–43 wt% (35–39 mol%). Additionally, the MgO promoted by (Li, Na, K)NO_3 showed relatively stable performance over 10 cycles.

3.1.3 Nitrites. The use of nitrites can be an alternative or complement to nitrate promoters. In addition to using nitrates, Harada *et al.*[86] promoted colloidal MgO nanoclusters with $LiNO_3$–(Na–K)NO_2. The nitrite-promoted MgO sorbent had a CO_2 uptake of 68.2 wt% (62.4 mol%) at 340 °C, with better cyclic stability than the MgO promoted by (Li–Na–K)NO_3 (Fig. 8). Zhao *et al.*[84] showed that using a mixture of nitrate and nitrite promoters can further enhance the performance of the hydrothermally synthesised MgO sorbents.[84] When 0–8 mol% $NaNO_2$ was doped to $NaNO_3$-promoted MgO (with molar ratio of $MgO : NaNO_3 = 1 : 0.07$) the CO_2 uptake increased from 66.9 wt% (61.3 mol%) to over 87 wt% (80 mol%), whilst showing stable performance over 15 cycles.

3.1.4 Carbonates. The presence of a carbonate promotor facilitate easier melting and faster CO_2 transport through the carbonate layer. Kwak *et al.*[87] employed a triple eutectic alkali carbonate (TEC) design, in which the MgO sorbent was promoted by a TEC mixture consisting of Li_2CO_3, Na_2CO_3, and K_2CO_3 (with a molar ratio of Li : Na : K of 0.435 : 0.315 : 0.250). They classified the CO_2 capture process into two steps: (1) "fast and large", and (2) "slow and small". The amount of TEC used affects the kinetics of these two steps differently – the rate of step 1 increases with increasing amount of TEC; but this was not observed for step 2. The optimal TEC amount was found to be 60 mol% (sample 60-TEC/MgO), which gave a CO_2 uptake of 43.4 wt% (39.7 mol%) in step 1 and an additional 33.9 wt% (31.0 mol%) in step 2. It was also found that MgO with low TEC content (20–40 mol%) had better cyclic stability than those with high TEC content (60–100 mol%).

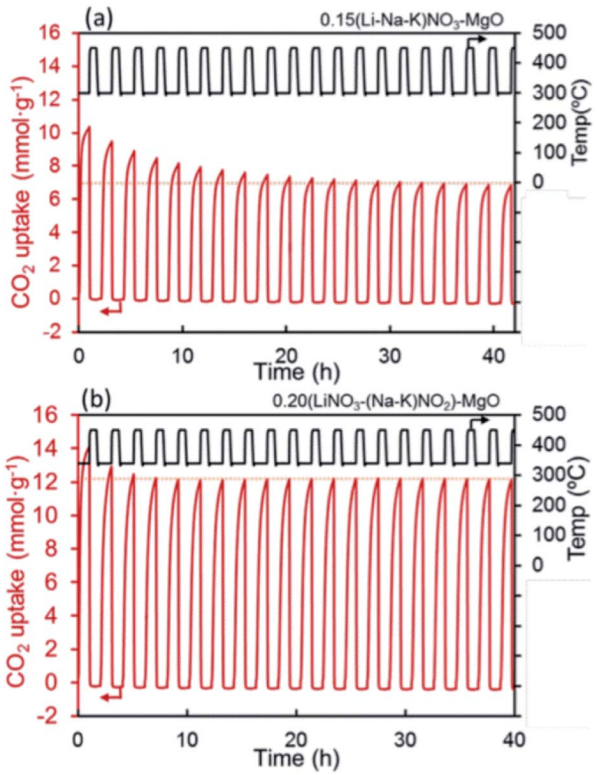

Fig. 8 CO_2 capture capacity of promoted MgO by alkali metal nitrates ((Li–Na–K)NO_3) and nitrate/nitrite ($LiNO_3$–(Na–K)NO_2) salt. Reprinted with permission[86] copyright 2021 American Chemical Society.

3.1.5 Carbonates with nitrite or nitrate. Co-Doping of carbonates and nitrates has been a popular approach for developing promoted MgO based sorbents,[83,88–91] with key studies summarised in Table 3. Here, we discuss key synthetic parameters governing the performance of the co-doped sorbents. Hwang *et al.*[83] investigated the doping of K_2CO_3 to $NaNO_3$ and KNO_3-promoted commercial MgO and found the K_2CO_3 : nitrate ratio to be important. Co-doping 30 wt% K_2CO_3 with 10 wt% of $NaNO_3$ or KNO_3 both worked well, rendering 44 wt% (40 mol%) uptake at 300 °C in 20 atm CO_2.[83] Vu *et al.*[91] promoted the performance of mesoporous MgO aerogels with double sodium salts ($MgO{\cdot}Na_2CO_3{\cdot}NaNO_3$). During operation, Na_2CO_3 and $NaNO_3$ facilitate a high concentration of O^{2-} in the molten salts, which would enhance the CO_2 capture capacity by accelerating the formation of $MgCO_3$. Furthermore, the molten salts hinder the

formation of the rate-limiting carbonate surface layers, whilst accelerating the production of CO_3^{2-}. Therefore, it is important to dope MgO with an optimal amount of alkali salts to maximise the benefit of eutectic formation. Specifically, the amount of Na_2CO_3 should be equal to or less than the amount of $NaNO_3$ for optimal CO_2 capture performance. According to Vu *et al.*, the highest CO_2 uptake of 56 wt% (51 mol%) was achieved at 325 °C (1 atm, pure CO_2) when the molar ratio of MgO : Na_2CO_3 : $NaNO_3$ was 1 : 0.05 : 0.2.[91] Wang *et al.*[92] also showed the benefit of having both nitrate and carbonate doped on MgO nano-sheets through a series of experiments and found that the optimal sorbent composition to be $[(LiNO_3, KNO_3)_2$–$(Na_2CO_3, K_2CO_3)]_{0.15}$/MgO, which showed a high CO_2 uptake of 73 wt% (67 mol%) (350 °C, 1 atm, 100% CO_2). They proposed a reaction mechanism between CO_2 and the sorbent, involving the following steps:

$$NO_3^- + K_2CO_3 + CO_2 \rightarrow NO_2^- + K_2C_2O_6 \quad (5)$$

$$K_2C_2O_6 + MgO \rightarrow K_2Mg(CO_3)_2 + 0.5O_2 \quad (6)$$

$$Na_2CO_3 + MgO + CO_2 \rightarrow Na_2Mg(CO_3)_2 \quad (7)$$

The finding of Wang *et al.*[92] was in agreement with Ding *et al.*,[88] who revealed that the reaction between CO_2 and MgO promoted with 10 mol% $[(Li_{0.44}K_{0.56})NO_3]_2[(Na_{0.5}K_{0.5})CO_3]$ takes place in three stages: (1) the formation of carbonate in the first 7 minutes – at this stage, CO_2 is dissolved in the molten salt and then reacts with MgO and formed a layer of carbonate (CO_3^{2-}), producing $K_2C_2O_6$ and $K_2Mg(CO_3)_2$. (2) The restriction of the rigid carbonate layer and the formation of the high concentration of oxygen ion within 10 minutes – oxygen ions (O^{2-}) are produced by the dissolution of MgO and the decomposition of the molten alkali nitrates and nitrites. (3) The nucleation of magnesium carbonate occurs between 10 and 60 minutes after contacting the CO_2.

3.2 Structured MgO sorbents

Morphological features, such as surface area, pore volume, size and thickness of the particle are all critical to the performance of MgO sorbents.[93] Therefore, researchers have explored various synthetic approaches to improve the morphological properties of MgO sorbents to enhance their CO_2 uptake.[94–96] In general, the CO_2 uptake correlates well to the sorbent's surface area. Guo *et al.*[94] showed that solid state chemical reaction (SR) method produced MgO with, smaller particle sizes, higher BET surface area (100 $m^2\ g^{-1}$), smaller pore sizes and higher pore volume (0.67 $cm^3\ g^{-1}$) than those produced by other synthesis methods, such as direct calcination (DC), direct precipitation (DP) and sol–gel (SG) – when $MgCl_2$ was used as the Mg precursor in all the synthesis methods. As a result, MgO synthesised by SR showed higher CO_2 uptake (10.5 wt%, 9.6 mol%) than those by the DC, DP and SG methods, which yielded CO_2 uptakes of 2.95–6.8 wt% (2.7–6.2 mol%). In addition, the CO_2 capture capacities are also correlated to the sorbents' basicity, which are classified as weak, medium and strong. Accordingly, the SR method yielded the highest number of medium and strong basic sites (responsible for 2.54 and 1.24 mmol CO_2 per g of uptake, respectively) as well as the highest total amount of basic sites (with a total uptake of 5.49 mmol CO_2 per g). The abundant basic sites enhanced the CO_2 uptake of the SR sorbent. Similarly, Ding *et al.*[95] showed that MgO synthesised from magnesium acetate tetrahydrate ($Mg(CH_3COO)_2$) and oxalic acid ($C_2H_2O_4$) dihydrate solution (MgO–MO) had a high BET surface area of 252 $m^2\ g^{-1}$, high pore volume of 0.763 $cm^3\ g^{-1}$ and CO_2 uptake capacity of 7.59 wt% (7.0 mol%) at 50 °C. The CO_2 uptake capacity of MgO–MO was superior compared to MgO synthesised by calcining magnesium carbonate (MgO–BMC), the rehydration of MgO–BMC (MgO–RF) and commercial MgO (MgO–CA).[95] Hanif *et al.*[96] found that MgO obtained by ammonia precipitation (AC) showed higher surface area (362 $m^2\ g^{-1}$, 0.701 $cm^3\ g^{-1}$) and CO_2 uptake 7.53 wt% (6.9 mol%) than those by urea hydrolysis (UC) and thermal degradation (TC).

Researchers have also developed porous MgO with structural regularities as a means to control the morphologies of the synthetic sorbents. The performance of the various MgO sorbents with well-defined morphologies is summarised in Fig. 9. Notable morphologies are discussed in details below (Fig. 10).

3.2.1 Sheets. Wang *et al.*[92] synthesised sheet-like $[(Li, K)_2$–$(Na, K)]_{0.15}$/MgO having a sheet thickness of ~40 nm. The MgO nanosheets showed higher CO_2 uptake than granular MgO because the former had more surface MgO, which can readily react with CO_2. This advantage is corroborated by the nanosheets' larger BET surface area (56 $m^2\ g^{-1}$), larger pore volume (0.24 $cm^3\ g^{-1}$) and larger mean pore diameter than the granular MgO. Additionally, the sheet-like MgO sorbents showed relatively stable performance over 20 cycles. CO_2 uptake capacity is summarised by the morphology with the surface area in Fig. 9.

3.2.2 Platelets. Hanif *et al.*[96] prepared both platelet, sheet-like and octahedra structured MgO sorbents. They found that platelet morphology shows larger BET surface area (362 $m^2\ g^{-1}$), higher pore volume (0.701 $cm^3\ g^{-1}$) and relatively higher CO_2 uptake of 7.53 wt% (6.9 mol%) than the other two morphologies.

3.2.3 Rods. Zhao *et al.*[84] and Tuan *et al.*[97] found rod-like MgO to perform better than other tested shapes such as MgO spheres (they are described as 'ball-like' in the original paper).

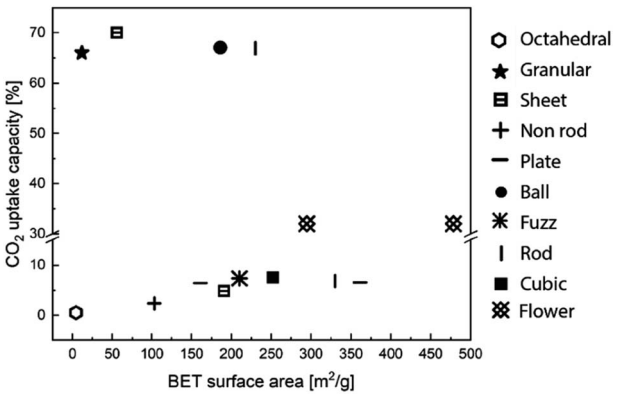

Fig. 9 CO_2 uptake capacity and BET surface area according to the various structure of MgO sorbents. The data points entries are obtained from ref. 84, 92, 95, 96, 98 and 99.

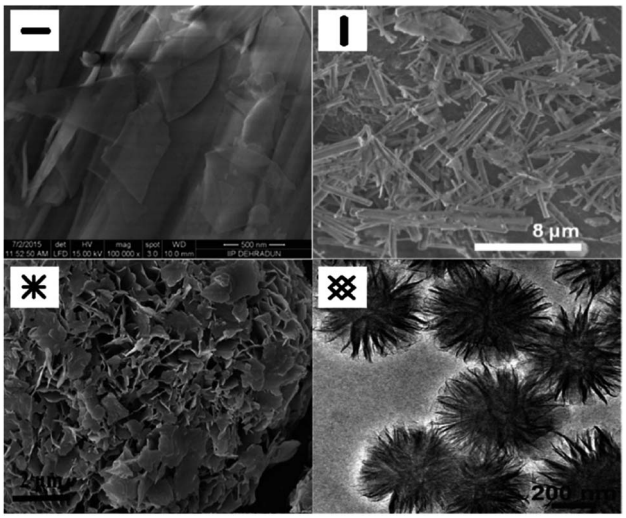

Fig. 10 SEM images of the structure of MgO sorbents: plate,[96] rod,[97] and fuzz-like structure of MgO sorbents[95] and TEM image of the flower-like plate,[98] Reprinted with permission copyright 2021 American Chemical Society.[96] Reprinted with permission copyright 2021 Royal Society of Chemistry,[95] Reprinted with permission copyright 2021 John Wiley and Son, Inc.[97,98]

Both teams attributed the enhanced CO_2 uptake by the rod-like MgO to their high BET surface area (230–331 $m^2\ g^{-1}$), larger pore volume (0.49–0.58 $cm^3\ g^{-1}$) as well as small particle sizes (~7 nm in both studies). CO_2 uptake capacity of rod-like MgO are drawn in Fig. 9.

3.2.4 Cubes. Cubic morphology may not be a trivial morphology that is typically associated with high specific surface areas. However, Ding *et al.*[95] reported a sorbent consisting of cube-like MgO grains with high BET surface area and pore volume (252 $m^2\ g^{-1}$, 0.76 $cm^3\ g^{-1}$). The MgO microcubes showed a CO_2 uptake capacity of 7.59 wt% (7.0 mol%), outperforming the plate-like MgO 6.44 wt% (5.9 mol%) prepared in the same study. Both of CO_2 uptake capacity are added in Fig. 9.

3.2.5 Flower. Li *et al.*[98,99] synthesised MgO/C composites with flower-like morphology. The large surface area and pore volume (295 $m^2\ g^{-1}$, 0.94 $cm^3\ g^{-1}$)[98] of the flower-like morphology facilitated efficient mass transport and improved the CO_2 uptake capacity of the MgO sorbents. Experimentally, the MgO/C nanocomposite showed a high CO_2 uptake of 30.9 wt% (28.3 mol%) at 27 °C, 1 bar. Using a similar synthetic strategy, Li *et al.*[100] combined the flowerlike MgO/C with the sheet-like graphene oxide and produced a sandwich-like structure with surface area (478 $m^2\ g^{-1}$) and pore volume (1.22 $cm^3\ g^{-1}$) even higher than the graphene oxide-free MgO/C nanocomposite. The sandwich-like structured showed an apparent uptake capacity of 31.5 wt% (28.8 mol%),[100] also plotted in Fig. 9.

3.3 Summary and knowledge gap

MgO based materials are promising CO_2 sorbents for applications at moderately high temperatures. When low-grade heat (<400 °C) is abundantly available on-site, using MgO to capture CO_2 may be more advantageous than calcium looping.[101] Additionally, MgO has the potential to become a highly effective CO_2 sorbent if its stoichiometric capture capacity can be fully exploited. In practice, the performance of MgO based sorbents is significantly hindered by its unfavourable carbonation mechanism and sluggish rates. Many different approaches have been studied to promote the uptake of CO_2 by MgO. Whilst high surface area, morphologically well-defined MgO sorbents could significantly improve CO_2 uptake, the experimentally accessible capacities are still substantially lower than the CaO based sorbents. Also, carbonation–calcination cycles could induce drastic morphological changes to the sorbents, making the morphologies of the freshly-prepared materials less relevant to the long-term performance.[102] Alternatively, the doping of alkaline metal salts to form low-melting eutectics is a much more effective to tackle the issue of the slow CO_2 uptake kinetics. However, the underlying science governing the promotional effects, including the interaction between the different salts in the eutectics, the interplay between different phases (*e.g.* molten salt, MgO and $MgCO_3$) and the mechanisms of ionic diffusion in the molten salt, must be further studied and better understood.[103] Lastly, many MgO sorbents suffer from poor cyclic stability. Therefore, further development is required to improve the effectiveness of the MgO based sorbents.

4 Li, Na, K, Sr and Ba based sorbents

As briefly discussed in Section 1, the carbonation of Li_2O, Na_2O, K_2O, SrO and BaO is practically irreversible. However, irreversible CO_2 sorbents are economically unattractive as they cannot be recycled and reused in continuous processes. Therefore, Li, Na, K, Sr and Ba based sorbents are often formulated as ternary oxides consisting of (i) at least one alkali metal or alkaline earth metal and (ii) at least one transition metal or semi-metal. The presence of transition metals and semi-metals introduces acidity to the ternary oxides and modulates the overall basicity of the sorbents, making them thermally regenerable at practically achievable temperatures. This section discusses the recent

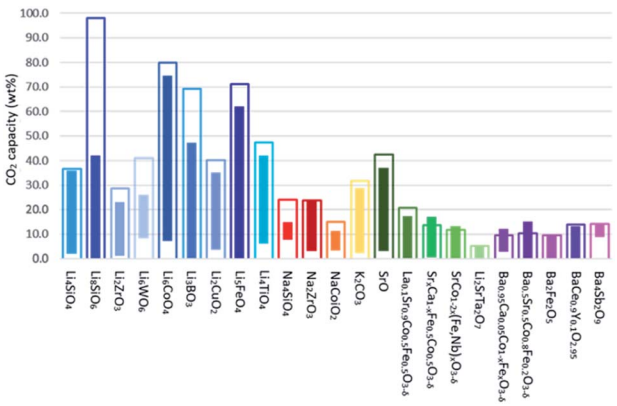

Fig. 11 Theoretical and experimental CO_2 uptake capacities of various Li-, Na-, K-, Sr- and Ba- based CO_2 sorbents. The hollow bars represent the stoichiometric capture capacities, whereas the solid bars represent the range of experimentally measured CO_2 uptakes. The sorbents are classified according to the chemical composition of the active components, *i.e.* excluding the formulation of the support.

Table 4 Various reaction conditions and capacities of Li, Na, K, Sr and Ba based sorbents[a]

Sorbent	Synthesis method	BET [$m^2\ g^{-1}$]	Stoichiometric CO_2 capacity [wt%]	Experimental CO_2 uptake [wt%]	Experimental CO_2 uptake [mol%]	Carbonation temperature [°C]	Calcination temperature [°C]	Carbonation CO_2 partial pressure [bar]	Calcination CO_2 partial pressure [bar]	Max no. of cycles	Ref.
Li_4SiO_4	a, b, c	0.06–10	36.7	1.8–36.0	4.9–98.1	RT-700[b]	550–900	0.04–1.0	0	250	114 and 116–121
Li_8SiO_6	a	—	98.0	0–42.0	0–42.9	25–776[b]	—	1.5	—	—	115
Li_2ZrO_3	a, b, c	2–3	28.7	0.01–23.0	0–80.1	500–575	600–700	0.10–2.0	0–0.585	30	122–124
Li_6WO_6	a	8	41.1	3.6–25.9	8.8–63.0	30–710[b]	730–760	0.60	0	4	130
Li_6CoO_4	a	1	80.0	5.0–76.4	6.3–95.5	300–700	700–750	0.20–1.0	0	10	127
Li_3BO_3	c, d	1–3	69.1	0–47.2	0–68.3	500–650	650	0.20–1.0	0	10	131
Li_2CuO_2	a, c	1–6	40.2	3.6–37.4	9.0–93.0	30–750[b]	750–850	1.0–5.0	0	—	128 and 129
Li_5FeO_4	a	—	71.2	0–62.0	0–87.1	30–700[b]	—	1.0	—	—	126
Li_4TiO_4	a	—	47.3	0–42.0	0–88.8	300–856	—	1.0	—	—	125
Na_4SiO_4	d	—	23.9	7.7–19.2	32.2–80.3	50–840[b]	—	0.80	—	—	133
Na_2ZrO_3	a, d	4–5	23.8	4.5–23.8	18.9–100.0	150–800	680–900	0.025–1.0	0	70	134–137
$NaCoO_2$	a	—	15.0	3.3–11.1	22.0–73.3	100–800	—	0.050–1.0	—	—	132
K_2CO_3	b, c, e	0.4–459	31.8	4.3–28.7	13.5–90.3	50–100	60–300	0.010–0.18	0–1.0	10	138–143
SrO	e	1–3	42.5	3.0–37.1	7.1–87.3	1100–1200	1100–1200	0.30–0.50	0	10	144
$La_{0.1}Sr_{0.9}Co_{0.5}Fe_{0.5}O_{3-\delta}$	f	—	20.7	0–17.3	0–83.6	600–800	—	0.10–1.0	—	—	145
$Sr_xCa_{1-x}Fe_{0.5}Co_{0.5}O_{3-\delta}$	f	—	27.3	0.4–17.0	1.5–62.3	RT-950[b]	—	1.0	—	—	146–148
$SrCo_{1-2x}(Fe, Nb)_xO_{3-\delta}$	a	—	23.6	0–13.1	0–55.5	925	—	0.75	—	—	149
$Li_2SrTa_2O_7$	—	—	5.1	0–4.9	0–96.1	140	700	—	—	6	151
$Ba_{0.95}Ca_{0.05}Co_{1-x}Fe_xO_{3-\delta}$	f	—	19.2	2.8–12.0	14.6–62.5	850	—	0.10	—	—	148
$Ba_{0.5}Sr_{0.5}Co_{0.8}Fe_{0.2}O_{3-\delta}$	a	—	20.9	0–14.9	0–71.4	RT-950[b]	—	1.0	—	—	149
$Ba_2Fe_2O_5$	a	—	18.8	0–9.4	0–50.0	1000	1000	1.0	0	—	153 and 154
$BaCe_{0.9}Y_{0.1}O_{2.95}$	a	—	13.8	0–13.1	0–94.9	600–1000	—	1.0	—	—	152
$Ba_4Sb_2O_9$	a	—	14.1	9.5–14.0	67.4–99.3	650–750	950	0.42	1	100	155

[a] Synthesis methods: (a) solid state; (b) impregnation suspension; (c) doping; (d) wet chemistry; (e) calcination; (f) citrate sol–gel method. [b] Indicates temperature programmed CO_2 capture experiments in a TGA.

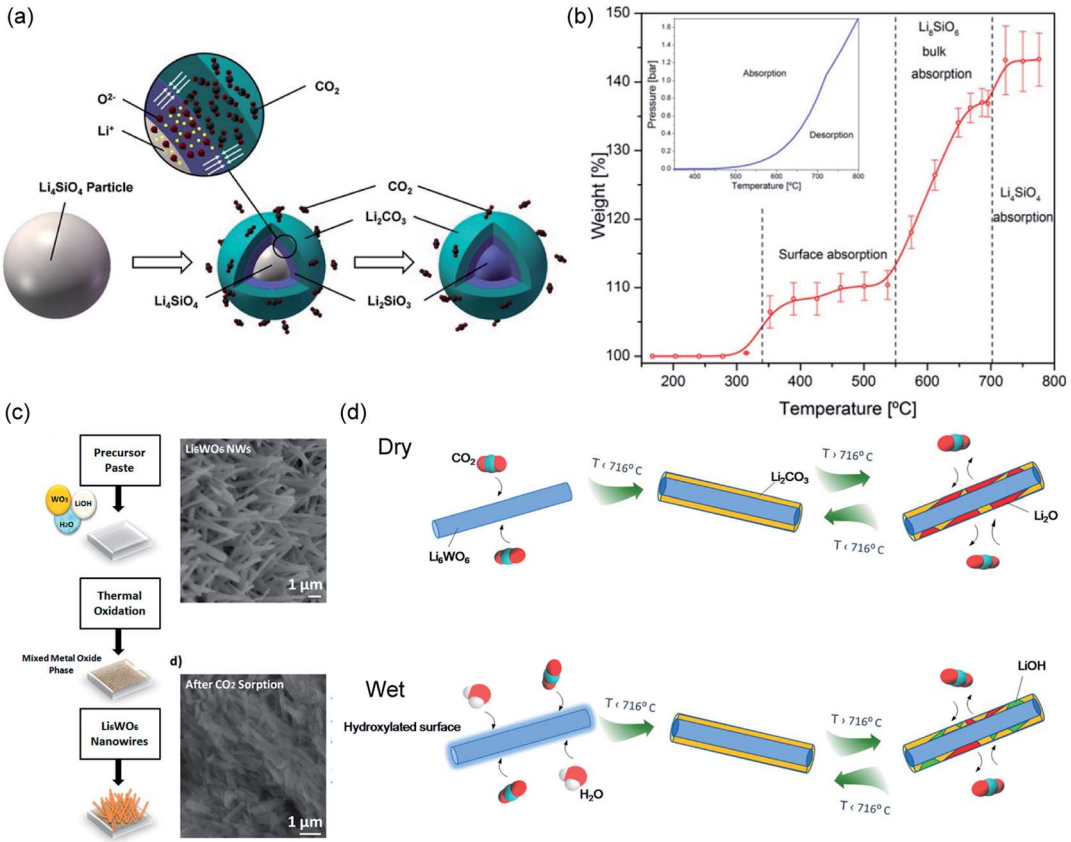

Fig. 12 (a) Schematic illustration of the "double shell" model describing Li_4SiO_4 carbonation. Reprinted with permission[114] copyright 2021 John Wiley and Son, Inc. (b) Temperature-programmed carbonation of Li_8SiO_6 in a TGA. Reprinted with permission[115] copyright 2021 American Chemical Society. (c) Illustration of synthesis of Li_6WO_6 NWs and its morphological change 30 min of carbonation at 700 °C. Reprinted with permission[91] copyright 2021 American Chemical Society. (d) Schematic illustration of CO_2 capture and release on Li_6WO_6 NWs under dry and wet conditions. Reprinted with permission[1] copyright 2021 American Chemical Society.

development in the formulation, synthesis and the CO_2 capture performance of synthetic Li, Na, K, Sr and Ba based sorbents. Fig. 11 summarises the stoichiometric and experimental CO_2 uptake capacities of the Li, Na, K, Sr and Ba based sorbents reported in the recent literature. A more elaborated summary is provided in Table 4.

4.1 Li based sorbents

4.1.1 Lithium silicates. Lithium silicates, including Li_4SiO_4 and Li_8SiO_6, are considered to be the most studied lithium based sorbents. The carbonation mechanism of these ternary oxides are fundamentally different from the CaO and MgO based ones, as more than one solid phases will form during carbonation. Li_4SiO_4 reacts with CO_2 between 450 and 700 °C with a stoichiometric CO_2 uptake capacity of 36.7 wt% according to:

$$Li_4SiO_4(s) + CO_2(g) \rightleftharpoons Li_2CO_3(s) + Li_2SiO_3(s) \quad (8)$$

The two solid products arrange themselves following a double-shell model, in which Li_2CO_3 and Li_2SiO_3 form an outer shell and an inner shell, respectively, as depicted in Fig. 12a.[114] The inner Li_2SiO_3 shell encapsulates the unreacted Li_4SiO_4 core. Once the shells have fully developed, further carbonation requires the migration of CO_2 inward through the Li_2CO_3 layer, and the migration of Li^+ and O_2^- ions outward through the Li_2SiO_3 layer. Therefore, the interface between Li_2CO_3 and Li_2SiO_3 is regarded as the reaction front, where new Li_2CO_3 forms. As both shells grow thicker, the diffusion resistance increases and slows down the rate. It is believed that the diffusion of CO_2 through the Li_2CO_3 layer is the rate limiting step, because the diffusion of CO_2 through the carbonate is considered slower than the diffusion of Li^+ and O_2^- through the silicate. Owing to the product layer diffusion resistances, the experimentally accessible uptake capacities are always lower than the stoichiometric values. For the chemically unmodified lithium silicates, the surface area of the sorbent becomes the effective rate limiting factor, which subsequently determines the practically achievable uptake capacity.

Using a lithium-richer compound such as Li_8SiO_6 could potentially improve the CO_2 uptake to 98 wt%. The carbonation of Li_8SiO_6 consists of 3 steps, as illustrated in Fig. 12b and confirmed by *in situ* synchrotron powder X-ray diffraction (SPXRD):[115]

Steps 1 and 2 involve the uptake of CO_2 by Li_8SiO_6 on the surface and in the bulk:

$$Li_8SiO_6(s) + 2CO_2(g) \rightleftharpoons 2Li_2CO_3(s) + Li_4SiO_4(s) \quad (9)$$

Step 3 involves the uptake of CO_2 by the formed Li_4SiO_4:

$$Li_4SiO_4(s) + CO_2(g) \rightleftharpoons Li_2CO_3(s) + Li_2SiO_3(s) \quad (10)$$

Lithium silicates can be easily synthesised by solid-state reactions. A typical synthesis involves mechanically mixing lithium and silicon precursors with desired stoichiometric ratios, followed by drying and calcination (at 800–900 °C). Typical lithium precursors include Li_2CO_3,[116,117] Li_2O (ref. 118) and $LiNO_3$,[119] whereas the silicon precursor is almost always SiO_2. Regardless of the precursor used, solid-state synthesised lithium silicates exhibit low specific surface areas (<1 m^2 g^{-1}) and low experimental CO_2 uptake capacities: 28–35 wt% (76–95 mol%) for Li_4SiO_4 (ref. 116 and 117) and 42 wt% (43 mol%) for Li_8SiO_6.[115] In addition, the poor sintering resistance of the solid product, Li_2SiO_3, results in rapid performance decay over CO_2 capture cycles.[117]

Given the dependence on product layer diffusion during carbonation, it is intuitive to prepare Li_4SiO_4 sorbents with high surface areas using wet chemistry methods such as impregnation suspension,[114,120] which involves mixing an aqueous solution of lithium precursors (*e.g.* lithium acetate and lithium lactate) with a SiO_2 sol suspension, which is subsequent dried and calcined.[114] Indeed, the resulting Li_4SiO_4 samples exhibit higher surface areas (1.6–2 m^2 g^{-1}), higher CO_2 uptake (up to 36 wt%, *i.e.* 98 mol%) and better cyclic durability (over 40 cycles) than those synthesised by solid-state reactions.[114]

Alternatively, the performance of Li_4SiO_4 can be improved by doping. Inert dopants (*e.g.* $CaCO_3$) can increase the sorbents' specific surface area and sintering resistance.[117] Low melting-point dopants, *e.g.* Na_2CO_3, K_2CO_3, $NaNO_3$ and KNO_3, can accelerate the transport of CO_2 through the Li_2CO_3 product layer, analogous to the case of alkali metal salt doped MgO sorbents.[119–121] Lastly, redox-active dopants, such as Fe^{3+}, can improve the transport of O^{2-} ions through the Li_2SiO_3 product layer.[118] Synthetically, doping can be achieved by including dopant precursors during the solid state synthesis of the Li_4SiO_4 sorbent,[116,117] impregnating the solid-state synthesised Li_4SiO_4 with soluble dopants (*e.g.* Na_2CO_3, K_2CO_3, $NaNO_3$ and KNO_3), or performing a secondary solid state reaction between the as-synthesised Li_4SiO_4 and the dopant precursor. Two-step solid state synthesis was used for the synthesis of $Li_{4+x}Si_{1-x}Fe_xO_4$ sorbents from Li_4SiO_4 and Li_5FeO_4.[118] As an economic and sustainable alternative, Wang *et al.* used acid-leached blast furnace slag, which contains TiO_2, Fe_2O_3, Al_2O_3, CaO and K_2O, as the silicon precursor for the solid-state synthesis of Li_4SiO_4.[116] The inherent presence of dopants in the silica precursor offers a cost-effective means to prepare high performance Li_4SiO_4 sorbents. In all cases, the dopant-promoted Li_4SiO_4 showed increased specific surface area (from 0.06 to 0.3 m^2 g^{-1}), improved CO_2 uptake (up to 35 wt%, *i.e.* 95 mol%),[117] improved cyclic stability (up to 250 cycles)[121] and faster rate of carbonation at low reaction temperatures in low CO_2 concentrations (in 20% CO_2 at 200 °C).[118]

4.1.2 Other Li based sorbents. Lithium zirconate (Li_2ZrO_3) is the second most studied lithium based sorbent with a stoichiometric uptake capacity of 28.7 wt%:

$$Li_2ZrO_3(s) + CO_2(g) \rightleftharpoons Li_2CO_3(s) + ZrO_2(s) \quad (11)$$

The experimentally reported carbonation temperatures are in the range of 450–650 °C. Similar to lithium silicates, the carbonation of Li_2ZrO_3 also proceeds *via* a double shell model, in which the inner and outer product layers are ZrO_2 and Li_2CO_3, respectively. The CO_2 diffusion through the Li_2CO_3 inner layer is considered to be the rate limiting step. Li_2ZrO_3 can be simply synthesised by solid-state reaction from Li_2CO_3 and ZrO_2. However, solid-state synthesised Li_2ZrO_3 show slow carbonation and low uptake capacities (5.9–10 wt%, *i.e.* 20.6–34.8 mol%).[122,123] Therefore, synthetic methods used to improve the performance of Li_4SiO_4 have also been adopted to promote the Li_2ZrO_3 sorbents, such as (i) doping low-melting point salts to improve the CO_2 mobility through the carbonate product layer,[123] (ii) doping redox-active Fe^{3+} to improve the O_2^-–CO_3^{2-} bi-ionic diffusivity through the Li_2CO_3 product layer,[122] and (iii) preparing Li_2ZrO_3–Na_2ZrO_3 solid–solution sorbents by impregnation suspension.[124] Methods (i) and (iii) appear to be more effective in enhancing CO_2 uptake (20–22 wt%, *i.e.* 70–77 mol%), whereas the improvement by Fe-doping is marginal (7.0–9.2 wt%, *i.e.* 24.4–32.1 mol%).

Ternary oxide phases containing Li and transition metals have also been prepared, primarily by solid-state synthesis, as CO_2 sorbents.[125–130] A summary of the carbonation chemistries of these Li-transition metal oxides is presented in Table 5. Amongst these ternary oxides, Li_6CoO_4 has both the highest stoichiometric CO_2 uptake and the highest experimental CO_2 uptake of 80.0 and 74.5 wt%, respectively,[127] whereas Li_6WO_6 nanowires showed the ability to rapidly capture CO_2 at ambient

Table 5 Summary of carbonation reactions of Li-transition metal-oxide materials

Active sorbent	Carbonation reactions	Stoichiometric CO_2 uptake capacity (wt%)
Li_4TiO_4	$Li_4TiO_4 + 4CO_2 = 4Li_2CO_3 + TiO_2$	41.5–47.3
Li_5FeO_4	$Li_5FeO_4 + 2CO_2 = LiFeO_2 + 2Li_2CO_3$ $LiFeO_2 + CO_2 = Li_2CO_3 + Fe_2O_3$	71.2
Li_6CoO_4	$Li_6CoO_4 + 3CO_2 = 3Li_2CO_3 + CoO$	80
Li_2CuO_2	$Li_2CuO_2 + CO_2 = Li_2CO_3 + CuO$	40.2
Li_6WO_6	$Li_6WO_6 + CO_2 = Li_4WO_5 + Li_2CO_3$ $Li_4WO_5 + CO_2 = Li_2WO_4 + Li_2CO_3$ $Li_2WO_4 + CO_2 = WO_3 + Li_2CO_3$	41.1

temperatures in the presence of moisture (relative humidity = 58 ± 3%). The high performance of Li_6WO_6 nanowires at ambient temperatures is attributed to the hydration and activation of the surface of the nanowires for accelerated carbonation, as illustrated in Fig. 12d.[127] For sorbents containing redox-active metals, *e.g.* Co and Fe, the redox environment during carbonation will also affect the CO_2 capture performance. For instance, the presence of O_2 promotes CO_2 uptake of Li_5FeO_4 by enhancing the ionic diffusion through the product layer.[118] In contrast, the performance of Li_6CoO_4 deteriorates quickly over cycles (76.4 wt%, *i.e.* 95.5 mol%, in the first cycle to 30.5 wt%, *i.e.* 38.1 mol% after 10 cycles), owing to the irreversible oxidation of Co^{2+} to Co^{3+} by the O_2 present under the testing conditions.[127]

The cyclic stability of Li-transition metal oxides is either poor or unreported. Doping a second transition metal (*e.g.* Mn, Fe or Ni)[128] and alkali metal nitrates (MNO_3, M = Li, Na, K)[129] has been proven effective for improving the capture capacity (from 23 wt% to 35 wt%, *i.e.* 57 to 87.1 mol%) and cyclic stability of Li_2CuO_2. Again, the improvement is by virtue of improving the ionic conductivity of the product layers.

Lastly, trilithium borate (Li_3BO_3) has been synthesised by precipitation using LiOH and H_3BO_3 as the precursors.[131] **Li_3BO_3** captures CO_2 with a stoichiometric uptake capacity of 41.4 wt%:

$$4Li_3BO_3 + 3CO_2 \rightleftharpoons 3Li_2CO_3 + Li_6B_4O_9 \quad (12)$$

With a reported experimental CO_2 uptake of 35.4 wt% (51.2 mol%), measured after 4 h in pure CO_2 at 580 °C. The poor cyclic stability of Li_3BO_3 could be improved by $NaNO_2$ or KNO_2 doping, which significantly accelerates product layer diffusion as the dopant salts form a molten layer. Interestingly, the 10 mol% (Na–K)NO_2 doped Li_3BO_3 showed an experimental uptake of 47.2 wt% (68.3 mol%), exceeding the stoichiometric maximum capacity predicted by eqn (16). This was because the alkali metal nitrites promoted the deep carbonation of lithium borate:

$$4Li_3BO_3 + 5CO_2 \rightleftharpoons 5Li_2CO_3 + Li_2B_4O_7 \quad (13)$$

$$Li_3BO_3 + CO_2 \rightleftharpoons Li_2CO_3 + LiBO_2 \quad (14)$$

Resulting in improved stoichiometric uptake capacities of 69.1 and 55.4 wt%, respectively.

4.2 Na based sorbents

Na based sorbents have similar chemical formulae as the Li based ones (see Section 4.1). Because sodium is earth-abundant, Na based sorbents are potentially more economical. On the other hand, sodium is heavier and therefore, the stoichiometric CO_2 uptake capacity of Na based sorbents are generally lower than that of the Li equivalents in terms of wt%. Experimentally, sodium orthosilicate, sodium zirconate and other sodium metal oxides have shown promising CO_2 capture performance over a wide temperature range (from near-ambient temperatures to 850 °C):

$$Na_4SiO_4 + CO_2 \rightleftharpoons Na_2CO_3 + Na_2SiO_3 \quad (15)$$

$$Na_2ZrO_3 + CO_2 \rightleftharpoons Na_2CO_3 + ZrO_2 \quad (16)$$

These compounds generally exhibit good cyclic stability, with the exception of undoped Na_2CoO_2:

$$Na_2CoO_2 + CO_2 \rightleftharpoons Na_2CO_3 + CoO, \quad (17)$$

which shows limited experimental CO_2 uptake (3.3–5.0 wt%, *i.e.* 22.0–33.3 mol%) that is substantially below the stoichiometric capacity of 15 wt%.[132]

Similar to Li based sorbents, Na based sorbents can be prepared by solid-state reactions between metal precursors, *e.g.* Na_2SiO_3 + NaOH,[133] Na_2CO_3 + ZrO_2,[134] and Na_2CO_3 + $CoCO_3$,[132] as well as by wet-chemistry methods such as sol–gel synthesis.[135,136]

Na_4SiO_4 was found to perform well above 750 °C, showing a maximum uptake of 19.2 wt% (80.3 mol%, with a stoichiometric uptake capacity of 23.9 wt%) at 840 °C.[133] One approach to improve the low-temperatures performance of Na_4SiO_4 is doping alkali carbonates (M_2CO_3, M = Li, Na, K), which promotes the diffusion of O_2^- through the molten carbonate layer. The promotional effects follow the order K_2CO_3 > Na_2CO_3 > Li_2CO_3, probably because of the increased basicity from Li to K.[133] Although the dopants decrease the mass-based CO_2 uptake capacity of the Na_4SiO_4 sorbent, doping significantly improved carbonation rates even below 700 °C. In particular, K_2CO_3-doped Na_4SiO_4 showed 4.7 wt% (19.7 mol%) CO_2 uptake at 300 °C, doubling that of undoped Na_4SiO_4.

During the carbonation of Na_2ZrO_3, the solid products could form a mesoporous layer with high gas permeability, as depicted in Fig. 13a and b. As a result, the Na_2ZrO_3 sorbents do not

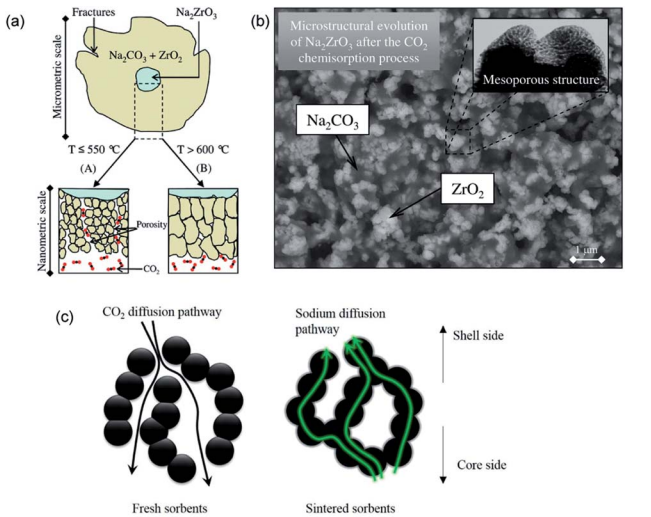

Fig. 13 (a) Scheme of the CO_2 uptake on Na_2ZrO_3 at different temperatures. Reprinted with permission[134] copyright 2021 American Chemical Society (b) SEM image of growth of ZrO_2 and Na_2CO_3 after the carbonation of Na_2ZrO_3. Reprinted with permission[134] copyright 2021 American Chemical Society (c) Scheme of the CO_2 and sodium diffusion in the sorbent under fresh and sintered state. Reprinted with permission[135] copyright 2021 Elsevier.

experience significant product layer diffusion resistance, as long as the product layer does not sinter.[137] Nevertheless, increasing the initial porosity of Na_2ZrO_3, *e.g.* by synthesising the sorbent using sol–gel method, could still render improvements in CO_2 uptake and cyclic stability during high temperature operations.[135] The best performance was achieved by the Na_2ZrO_3 prepared from sodium oxalate and $Zr(NO_3)_4$, showing an uptake of 22.6 wt% (95.0 mol%, with a stoichiometric uptake of 23.8 wt%), which was largely maintained over 5 successive cycles. Ji *et al.* attributed the high performance to the partly sintered product layer, which facilitates fast sodium diffusion as a form of mass transfer enhancement, as depicted in Fig. 13c.

For $NaCoO_2$, substitutionally doping the Co sites with Fe could substantially improve the redox activity, ionic conductivity and therefore CO_2 capture performance of the ternary oxide. For instance, $NaCo_{0.7}Fe_{0.3}O_2$ showed improved capacity of 10.6 wt% (70.7 mol%) in 20% CO_2 at 700 °C (*cf.* 3.3 wt%, 22.0 mol% without doping).[132] The CO_2 uptake could be further improved to 11.1 wt% (74.0 mol%) in the presence of 5% O_2 at 800 °C, because the presence of O_2 would stabilise the $NaCoO_2$ phase.

4.3 K based sorbents

Unlike lithium and sodium based sorbents, whose functional forms are mixed oxides, potassium based sorbents primarily function in the form of K_2CO_3 and take up CO_2 by forming bicarbonate in the presence of moisture with a stoichiometric CO_2 uptake capacity of 31.8 wt%:

$$K_2CO_3 + CO_2 + H_2O \rightleftharpoons 2KHCO_3 \quad (18)$$

Experimentally, the carbonation and regeneration of K_2CO_3 occur at 50–60 °C and around 200 °C, respectively. This makes K_2CO_3 an excellent candidate for CO_2 capture at near-ambient temperatures. The practically achievable CO_2 uptake by K_2CO_3 is as high as 28.7 wt% (90.3 mol%).[138] However, the cyclic stability of K_2CO_3 is limited.

To improve the cyclic stability, researchers have impregnated K_2CO_3 on various types of high melting point supports. The most readily available support material is alumina.[139] However, the interaction between Al_2O_3 and K_2CO_3 would form the thermally stable $KAl(CO_3)(OH)_2$:[140]

$$K_2CO_3 + Al_2O_3 + CO_2 + 2H_2O \rightleftharpoons KAl(CO_3)(OH)_2, \quad (19)$$

which results in drastic capacity loss (9.6 wt%, to 4.8 wt%, *i.e.* 30.2 mol% to 15.1 mol%) after only 3 cycles.[141] One way to avoid $KAl(CO_3)(OH)_2$ formation is to restrict the operation to ambient temperatures and perform pressure swing cycles instead.[142] However, the cost-benefit of doing pressure swing CO_2 capture must be further justified, as pressure swing processes are often associated with high energy penalties and additional costs arising from gas compression.

Alternatively, support materials that do not react with K_2CO_3 can be used, such as silicates (*e.g.* $Al_6Si_2O_{13}$, $CaSiO_3$, $ZrSiO_4$, which inert towards K_2CO_3),[141] ZrO_2 (ref. 139) and porous carbon.[143] In all cases, stable performance over 10 cycles can be achieved at the expense of reduced CO_2 uptake (6.5–11.8 wt%, *i.e.* 20.4–37.1 mol% *cf.* the stoichiometric maximum of 31.8 wt%). Most interestingly, Yang *et al.*[143] impregnated K_2CO_3 on carbon aerogels, which possess extremely specific high surface areas (350 to 450 $m^2\ g^{-1}$) and provide additional physisorption sites for CO_2. As a result, they reported the highest CO_2 uptake of 9.2–11.8 wt% (28.9–37.1 mol%), amongst the highest of all supported K_2CO_3 sorbents. Nevertheless, the

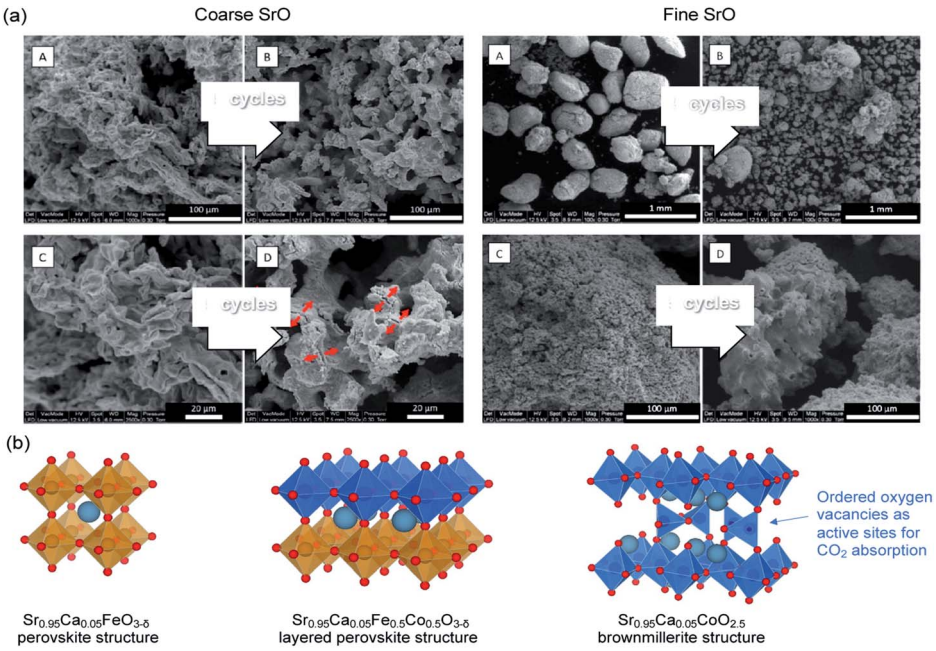

Fig. 14 (a) SEM images of coarse and fine SrO particles before (A & C) and after five cycles (B & D) of carbonation–calcination at 1100 °C (b) $Sr_{0.95}Ca_{0.05}Fe_{0.5}Co_{0.5}O_{3-\delta}$ perovskite with a layered structure and its phase segregation to a Fe-rich and a Co-rich phase. The undercoordinated Co sites are considered to be the preferential sites for CO_2 absorption. Reprinted with permission[144] copyright 2021 American Chemical Society.

application of the carbon based supports for CO_2 capture must be further validated under realistic operation conditions, considering the lack of CO_2 selectivity by the physisorption process and the lack of stability of carbon in the presence of oxygen, a common component in combustion flue gases.

4.4 Sr based sorbents

SrO can function by itself as a high temperature (>1000 °C) CO_2 sorbent with relatively high initial CO_2 uptake. Indeed, Miccio *et al.*[144] prepared SrO sorbents with mean particle size of 0.5 mm and 5.0 mm by calcining $SrCO_3$ and wet-granulation (Fig. 14a). The SrO sorbents with mean particle size of 0.5 mm and 5.0 mm had specific surface areas of 1.3 and 2.2 $m^2\ g^{-1}$, respectively.[144] Both the fine, low surface area and coarse, high surface area SrO particles showed high initial CO_2 uptake capacities of 37.1 and 30.5 wt% (87.3 and 48.2 mol%), respectively, when tested in 50% CO_2 at 1100 °C. However, the uptake capacity rapidly dropped over cycles due to sintering. The attempt to support SrO_2 on Al_2O_3 by mechanical mixing resulted in the formation of $Sr_3Al_2O_6$ and $SrAl_2O_4$, both appeared beneficial to the sorbent's cyclic stability, at the expense of reducing the capture capacity to 8.7–9.3 wt% (20.5–21.9 mol%).

Alternatively, Sr-containing perovskites, in which Sr occupies the A sites in the ABO_3 lattice, can be used directly as CO_2 sorbents. These perovskite structured sorbents are typically prepared *via* sol–gel synthesis.[145] The A site and B site occupancies of the perovskites can be flexibly adjusted by varying the compositions of the metal precursors during the sol–gel synthesis. The site occupancies in turn influence the CO_2 capture performance. For example, $La_{0.1}Sr_{0.9}Co_{0.5}Fe_{0.5}O_{3-\delta}$ was found to capture more CO_2 (17.3 wt%, *i.e.* 83.6 mol%) than $Sr_{0.95}Ca_{0.05}Fe_{0.5}Co_{0.5}O_{3-\delta}$ (4.48 wt%, *i.e.* 18.3–33.2 mol%).[146,147] However, further increasing the Ca occupancy in the A site (replacing more Sr) to $Sr_{0.5}Ca_{0.5}Fe_{0.5}Co_{0.5}O_{3-\delta}$ could improve the uptake to 17 wt% (62.3 mol%).[147] Such improvement was attributed to the fact that $Sr_{0.5}Ca_{0.5}Fe_{0.5}Co_{0.5}O_{3-\delta}$ with $\delta \approx 0.53$ corresponds to a brownmillerite structure (see Fig. 14b) with ordered oxygen vacancies, which are regarded by many to be beneficial to CO_2 uptake:[146,148]

$$2(Sr, Ca)(Fe, Co)O_{2.5} + CO_2 \rightleftharpoons (Sr, Ca)CO_3 + (Sr, Ca)(Fe, Co)_2O_4 \quad (20)$$

Adjusting the B-site occupancies could also influence the capture performance. Lu *et al.*[149] synthesised $SrCo_{1-2x}(Fe, Nb)_xO_{3-\delta}$ with equimolar amount of Fe and Nb by solid-state reactions between $SrCO_3$, Co_3O_4 (or Co_2O_3), Fe_2O_3, and Nb_2O_5. For $x = 0.05$ and 0.10, the freshly synthesised sorbents showed CO_2 uptake of 13.1 wt% (55.5 mol%) and 11.1 wt% (47.0 mol%), respectively, when evaluated in 75% CO_2 at 925 °C. Here, the increased B site occupancy by Nb enhanced the acidity and reduced the activity of the perovskite towards carbonation.[150]

Beyond the cubic-perovskite structure, a Ruddlesden–Popper (RP) structured ($A'_2[A_{n-1}B_nO_{3n+1}]$) $Li_2SrTa_2O_7$ sorbent was prepared by Galven *et al.* by solid state synthesis.[151] This RP phase achieved 4.90 wt% (96.1 mol%) uptake (with a stoichiometric uptake of 5.11 wt%) after 15 h in humid CO_2 at 140 °C, 30 bar pressure:

$$Li_2SrTa_2O_7 + 0.5CO_2 + 0.5H_2O \rightleftharpoons LiHSrTa_2O_7 + 0.5Li_2CO_3 \quad (21)$$

In addition, the $Li_2SrTa_2O_7$ sorbent exhibited excellent cyclability with negligible capacity loss over 6 cycles of isothermal carbonation at 140 °C and regeneration up to 700 °C. Such performance merits further development and investigation.

4.5 Ba based sorbents

Like Sr based sorbents, most studies on Ba based sorbents focus on the use of perovskite-type oxides with Ba occupying the A sites. These Ba based perovskites can be prepared by either sol–gel synthesis[148] or solid state reactions.[152] Likewise, the performance of the Ba based sorbents also depends on the site occupancies. For example, Nomura *et al.*[148] found that changing the Fe occupancy in $(Ba_{0.95}Ca_{0.05})(Co_{1-x}Fe_x)O_{3-\delta}$ from 0.2 to 0.9 resulted in a reduction in CO_2 uptake from 10.0 wt% (52.5 mol%) to 8.7 wt% (45.3 mol%). Given that $BaFeO_{3-\delta}$ ($0 < \delta < 0.5$) type materials are capable of reversibly changing phase between perovskite (ABO_3) and brownmillerite ($A_2B_2O_5$), facilitated by oxygen uptake and release, their CO_2 capture performance would also dependent on the oxygen partial pressure and the temperature. In general, unstable $BaFeO_{3-\delta}$ structures correspond to improved CO_2 capture performance. For example, carbonating $Ba_{0.95}Ca_{0.05}Co_{0.8}Fe_{0.2}O_{3-\delta}$ in the absence of oxygen renders an improved capture capacity of 12 wt% (62.5 mol%), owing to the thermal decomposition of perovskite to brownmillerite, which appeared as a better sorbent; this finding is in agreement with Lu *et al.*[149] and Fujishiro *et al.*[153] Yi *et al.* doped the B-sites of $BaFeO_{3-\delta}$ with Nb,[154] and reported low CO_2 uptake (1.3 wt%, 6.9 mol%) of the doped perovskite. We suspect that the Nb dopant donates electrons to the perovskite structure, which becomes chemically stabilised and unreactive towards CO_2. The most outstanding Ba based sorbents is perhaps the 6H-perovskite $Ba_4Sb_2O_9$ reported by Dunstan *et al.*[155] The authors prepared the sorbents by solid-state reaction between $BaCO_3$ and Sb_2O_3. $Ba_4Sb_2O_9$ reacts with CO_2 with a stoichiometric CO_2 uptake capacity of 14.1 wt%:

$$Ba_4Sb_2O_9 + 3CO_2 \rightleftharpoons BaSb_2O_6 + 3BaCO_3 \quad (22)$$

Experimentally, near-stoichiometric CO_2 uptake of 13.75 wt% (99.3 mol%) was observed upon carbonation at 750 °C. During long-term cyclic operation, $Ba_4Sb_2O_9$ showed >10 wt% (70.9 mol%) CO_2 uptake over 100 uptake–regeneration cycles (Fig. 15a). The excellent cyclic stability of $Ba_4Sb_2O_9$ originated from the sorbent's ability to fully regenerate its complete pore structure in each cycle, despite the fact that the fully carbonated sorbent showed virtually no porosity (Fig. 15b). The same authors also found $Ba_4Nb_{2-x}Ta_xO_9$ materials to be poor CO_2 sorbents, showing uptake <0.07 wt% in 100% CO_2 at up to 1000 °C.[156]

4.6 Summary and knowledge gap

Compared to the CaO and MgO based sorbents, Li, Na, K, Sr and Ba based sorbents are less commonly studied. Owing to the

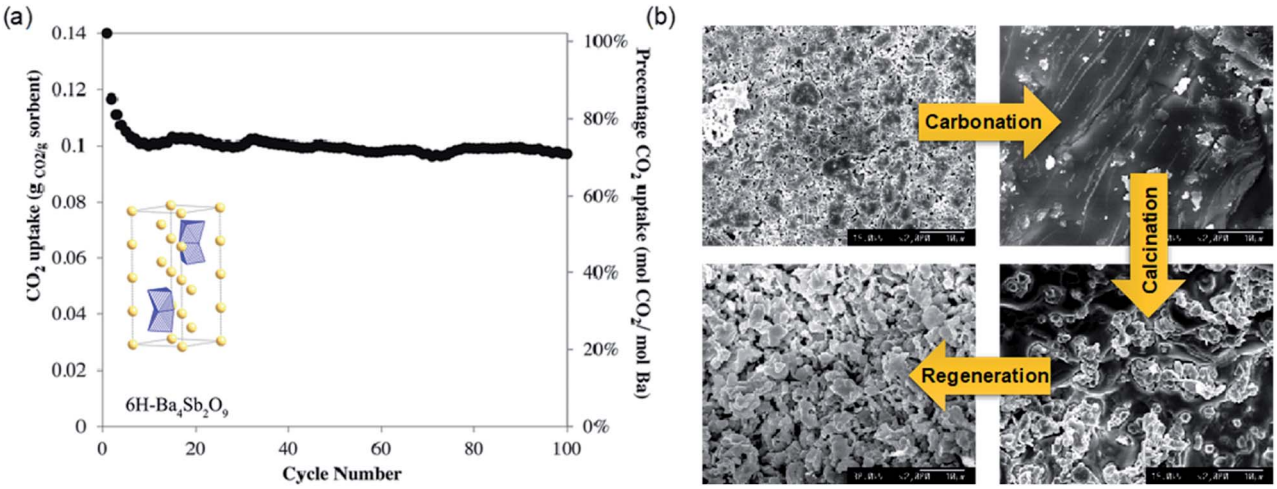

Fig. 15 (a) CO_2 uptake by 6H perovskite $Ba_4Sb_2O_9$ over 100 carbonation–calcination cycles in at TGA. (b) Surface morphology $Ba_4Sb_2O_9$ as it evolves over carbonation–calcination cycles. Reprinted with permission[155] copyright 2021 American Chemical Society.

high alkalinity of the metal sites, Li, Na, K, Sr and Ba based oxides require chemical modifications to function as reversible CO_2 sorbents at reasonable temperatures. These chemical modifications refer to a large pool of candidate sorbent compositions. Whilst many of these sorbents behave similarly during CO_2 uptake (*e.g.*, the double shell model for lithium silicates, lithium zirconates, sodium silicates and sodium zirconates), significantly more research is needed to fully understand and rationalise the behaviour of these mixed oxide sorbents in relation to their chemical composition, structure and synthesis methods. Following the discussion above, we summarise the following knowledge gaps for Li, Na, K, Sr and Ba based sorbents:

- The effect of strain development on the product layers during carbonation (*e.g.* following the double shell model depicted in Fig. 12a) is not well understood.
- Most of the sorbents discussed in this section have not been tested under practical CO_2 capture conditions, *i.e.* carbonation in 5–15% CO_2 (in the presence of moisture) and calcination in pure CO_2.
- The test conditions employed by different studies are inconsistent, making it difficult to make fair comparisons.
- Most CO_2 uptake tests were done in TGA, whilst some sorbents have only been studied for 1 carbonation cycle or by temperature programme carbonation.
- The synthesis parameters have not be sufficiently explored to identify optimal synthesis procedures.
- The cost-benefit of synthesising sorbents with complex structures and compositions must be justified.

5 Challenges and opportunities

This review discusses the recent advances in developing synthetic oxide sorbents for CO_2 capture. The CO_2 uptake ability of these sorbents originates from the alkalinity of the group 1 and group 2 metals. Because of reasons associated with cost, natural abundance and the performance of the natural mineral-derived sorbents, different classes of solid oxide sorbents have received varying extents of research attention and have reached different levels of technological maturity. Specifically, CaO based sorbents can be produced at large quantities from low-cost Ca sources (*e.g.* limestone), and have been extensively tested over a wide range of scales (from TGA to pilot plants) in realistic flue gas compositions. In contrast, all non-CaO based sorbents require specific chemical modifications to achieve improved CO_2 capture kinetics and capacity. Furthermore, the lack of testing standards for the non-CaO sorbents makes it difficult to have meaningful comparisons between different studies, even if they report similar chemical formulations. Addressing the lack of testing standards with priority will allow the field to develop faster and more efficiently.

There is also much commonality between different classes of sorbents. For instance, the carbonation of almost all solid oxide sorbents depends on the porosity and the mass transfer through the carbonated product layer. However, maintaining the porous structure of a solid material while it undergoes many cycles of phase changes (*i.e.* between oxides and carbonates) is technically challenging. Indeed, much research has been devoted to improving the cyclic stability of the solid oxide sorbents through synthetic approaches. One of the key methods involves mixing the active sorbent phases with thermal stabilisers such as Al_2O_3 and ZrO_2. Here, the chemical interaction between the active component (solid bases) and the thermal stabilizer phases (typically acidic oxides) must be understood and taken into consideration, as these interactions could potentially form inert phases (*e.g.* $Ca_{12}Al_{14}O_{33}$ and $KAl(CO_3)(OH)_2$) to dilute the CO_2 uptake capacity of the composite sorbents.

The synthetic approaches to improve the CO_2 uptake kinetics are also equally applicable across different classes of sorbents. For example, doping the sorbent surface with low-melting point salts could result in the formation of a molten salt layer during high temperature operation. Consequently, the mass transfer of CO_2 through the carbonate product layer can be drastically improved. Doping redox active metals such as Fe^{3+} could further

enhance the mass transfer, which is governed by ionic diffusion through the molten layer, thereby achieving fast CO_2 capture and high CO_2 uptake capacity. For sorbents that do not rely on the functioning of the molten salt layer, it is generally beneficial to prepare sorbents with high specific surface area and high porosity. To this end, the knowledge in preparing CaO based sorbents, *e.g.* the effect of synthesis parameters on the morphological properties of the final products, can be adapted for improving the performance of other types of oxide sorbents for a wide range of process applications.

For applications where the capturing and regeneration should take place at moderate to low temperatures, there is also an opportunity to hybridise metal oxides with membranes, polymers, and carbon-based materials to yield synergistic effects and enhanced sorbent performance.[157–159] For instance, it has been reported that doping membranes with metal oxides resulted in improved CO_2 uptake. Doped membranes with polar –OH group on the surfaces can increase the membrane sorbent's reactivity with CO_2 molecules – as CO_2 molecules and metal oxide act as electron acceptors and donors, respectively, the selectivity and permeability of the oxide-doped membrane towards CO_2 molecules can be effectively increased.[160–162] On the other hand, more research effort is required to improve the cyclic regenerability and durability of these composite sorbent materials.

Beyond experimental approaches, the emerging of computational chemistry has offered opportunity to accelerate sorbent formulation with unprecedented efficiencies. In fact, computational approaches have been widely adopted by chemists developing solid sorbents based on MOFs, zeolites and carbon materials,[163–166] including high-throughput screening studies that explored candidate sorbent materials in computational databases.[167–170] For solid oxide sorbents, *ab initio* computational studies would in the first instance rely on density functional theory (DFT) calculations to predict the properties of the oxides and the active sites for CO_2 uptake. Dunstan *et al.* has conducted a pioneering high throughput screening of oxidic CO_2 sorbent materials using the Materials Project database and identified Na_3SbO_4 and Li_5FeO_4 to be promising CO_2 sorbents.[19] Similarly, the computational screening by Gaultois *et al.* found Li_5SbO_5 as a potential sorbent, which showed satisfactory CO_2 uptake performance (~72% of its stoichiometric uptake capacity) over 25 cycles.[130] At present, there remains a gap between the thermochemical material properties that are computationally predicted and those experimentally measured. Such gap could potentially hinder the effective of the computational approaches to discover and develop new sorbents. However, with the rapid advancement in computational methods to simulate detailed chemical and physical phenomena, we anticipate computer-aided materials design methods to play major roles in the future development of solid oxide CO_2 sorbents.

Author contributions

Ribooga Chang: data curation, formal analysis, writing – original draft, writing – review & editing; Xianyue Wu: data curation, formal analysis, writing – original draft, writing – review & editing; Ocean Cheung: conceptualization, funding acquisition, supervision, writing – review & editing; Wen Liu: conceptualization, funding acquisition, supervision, writing – review & editing.

Conflicts of interest

There are no conflicts to declare.

Acknowledgements

R. C. and O. C. thank the Swedish Foundation for International Cooperation in Research and Higher Education (STINT) (Grant no. IB2019-8184), the Swedish Research Council (Grant no. 2020-04029) and Swedish Research Council for Sustainable Development (FORMAS, Grant no. 2018-00651) for their financial support. W. L. acknowledges the financial support by National Research Foundation of Singapore under its Campus of Research Excellence and Technological Enterprise (CRETE) programme.

References

1 M. Z. Akram, V. Atla, A. Nambo, B. P. Ajayi, J. B. Jasinski, J. He, J. R. Gong and M. Sunkara, *Nano Lett.*, 2018, **18**, 4891–4899.
2 G. D. Farquhar, M. L. Goulden, M. J. R. Fasham, M. Heimann, V. J. Jaramillo, H. S. Kheshgi, C. Le Quéré, R. J. Scholes and D. W. R. Wallace, *IPCC*, 2001.
3 M. Bui, C. S. Adjiman, A. Bardow, E. J. Anthony, A. Boston, S. Brown, P. S. Fennell, S. Fuss, A. Galindo, L. A. Hackett, J. P. Hallett, H. J. Herzog, G. Jackson, J. Kemper, S. Krevor, G. C. Maitland, M. Matuszewski, I. S. Metcalfe, C. Petit, G. Puxty, J. Reimer, D. M. Reiner, E. S. Rubin, S. A. Scott, N. Shah, B. Smit, J. P. M. Trusler, P. Webley, J. Wilcox and N. Mac Dowell, *Energy Environ. Sci.*, 2018, **11**, 1062–1176.
4 R. Stanger, T. Wall, R. Spörl, M. Paneru, S. Grathwohl, M. Weidmann, G. Scheffknecht, D. McDonald, K. Myöhänen, J. Ritvanen, S. Rahiala, T. Hyppänen, J. Mletzko, A. Kather and S. Santos, *Int. J. Greenhouse Gas Control*, 2015, **40**, 55–125.
5 M. Finkenrath, *Chem. Eng. Technol.*, 2012, **35**, 482–488.
6 A. Brunetti, F. Scura, G. Barbieri and E. Drioli, *J. Membr. Sci.*, 2010, **359**, 115–125.
7 F. Vega, A. Sanna, B. Navarrete, M. M. Maroto-Valer and V. J. Cortés, *Greenhouse Gases: Sci. Technol.*, 2014, **4**, 707–733.
8 S. Kumar, R. Srivastava and J. Koh, *J. CO2 Util.*, 2020, **41**, 101251.
9 Z. Hu, Y. Wang, B. B. Shah and D. Zhao, *Adv. Sustainable Syst.*, 2019, **3**, 1800080.
10 O. Cheung and N. Hedin, *RSC Adv.*, 2014, **4**, 14480–14494.
11 M. Ding, R. W. Flaig, H.-L. Jiang and O. M. Yaghi, *Chem. Soc. Rev.*, 2019, **48**, 2783–2828.

12 O. K. Farha, A. Özgür Yazaydın, I. Eryazici, C. D. Malliakas, B. G. Hauser, M. G. Kanatzidis, S. T. Nguyen, R. Q. Snurr and J. T. Hupp, *Nat. Chem.*, 2010, **2**, 944–948.
13 L. H. Xie, M. M. Xu, X. M. Liu, M. J. Zhao and J. R. Li, *Adv. Sci.*, 2020, **7**, 1901758.
14 S. Mukherjee, S. Sharma and S. K. Ghosh, *APL Mater.*, 2019, **7**, 050701.
15 N. Ghasem, in *Advances in Carbon Capture*, 2020, pp. 479–501.
16 C. Song, Q. Liu, S. Deng, H. Li and Y. Kitamura, *Renewable Sustainable Energy Rev.*, 2019, **101**, 265–278.
17 G. Ji and M. Zhao, *Recent Advances in Carbon Capture and Storage*, 2017, ch. 3, DOI: DOI: 10.5772/65723.
18 U. W. R. Siagian, A. Raksajati, N. F. Himma, K. Khoiruddin and I. G. Wenten, *J. Nat. Gas Sci. Eng.*, 2019, **67**, 172–195.
19 M. T. Dunstan, A. Jain, W. Liu, S. P. Ong, T. Liu, J. Lee, K. A. Persson, S. A. Scott, J. S. Dennis and C. P. Grey, *Energy Environ. Sci.*, 2016, **9**, 1346–1360.
20 J. Blamey, E. J. Anthony, J. Wang and P. S. Fennell, *Prog. Energy Combust. Sci.*, 2010, **36**, 260–279.
21 C. C. Dean, J. Blamey, N. H. Florin, M. J. Al-Jeboori and P. S. Fennell, *Chem. Eng. Res. Des.*, 2011, **89**, 836–855.
22 M. Reitz, M. Junk, J. Ströhle and B. Epple, *Int. J. Greenhouse Gas Control*, 2016, **54**, 272–281.
23 J. A. Duffy, *J. Am. Ceram. Soc.*, 1997, **80**, 1416–1420.
24 J. A. Duffy, *Geochim. Cosmochim. Acta*, 1993, **57**, 3961–3970.
25 J. Wang, L. Huang, R. Yang, Z. Zhang, J. Wu, Y. Gao, Q. Wang, D. O'Hare and Z. Zhong, *Energy Environ. Sci.*, 2014, **7**, 3478–3518.
26 M. T. Dunstan, F. Donat, A. H. Bork, C. P. Grey and C. R. Müller, *Chem. Rev.*, 2021, **121**, 12681–12745.
27 A. Perejón, L. M. Romeo, Y. Lara, P. Lisbona, A. Martínez and J. M. Valverde, *Appl. Energy*, 2016, **162**, 787–807.
28 M. C. Romano, I. Martínez, R. Murillo, B. Arstad, R. Blom, D. C. Ozcan, H. Ahn and S. Brandani, *Energy Procedia*, 2013, **37**, 142–150.
29 A. M. Kierzkowska, R. Pacciani and C. R. Muller, *J. Mater. Chem. A*, 2013, **6**, 1130–1148.
30 T. Xu, X. Wang, B. Xiao and W. Liu, *Chem. Eng. J.*, 2021, **425**, 131522.
31 IEA, *The challenge of reaching zero emissions in heavy industry*, IEA, Paris, 2020, https://www.iea.org/articles/the-challenge-of-reaching-zero-emissions-in-heavy-industry.
32 S. Gardarsdottir, E. De Lena, M. Romano, S. Roussanaly, M. Voldsund, J.-F. Pérez-Calvo, D. Berstad, C. Fu, R. Anantharaman, D. Sutter, M. Gazzani, M. Mazzotti and G. Cinti, *Energies*, 2019, **12**, 542.
33 M. C. Romano, M. Spinelli, S. Campanari, S. Consonni, G. Cinti, M. Marchi and E. Borgarello, *Energy Procedia*, 2013, **37**, 7091–7099.
34 B. Arias, M. E. Diego, J. C. Abanades, M. Lorenzo, L. Diaz, D. Martínez, J. Alvarez and A. Sánchez-Biezma, *Int. J. Greenhouse Gas Control*, 2013, **18**, 237–245.
35 M.-H. Chang, W.-C. Chen, C.-M. Huang, W.-H. Liu, Y.-C. Chou, W.-C. Chang, W. Chen, J.-Y. Cheng, K.-E. Huang and H.-W. Hsu, *Energy Procedia*, 2014, **63**, 2100–2108.
36 B. Arias, M. Alonso and C. Abanades, *Ind. Eng. Chem. Res.*, 2017, **56**, 2634–2640.
37 M. Erans, M. Jeremias, V. Manovic and E. J. Anthony, *J. Visualized Exp.*, 2017, **128**, e56122.
38 A. de la Calle Martos, J. M. Valverde, P. E. Sanchez-Jimenez, A. Perejon, C. Garcia-Garrido and L. A. Perez-Maqueda, *Phys. Chem. Chem. Phys.*, 2016, **18**, 16325–16336.
39 C. Zhongxiang, H. S. Song, M. Portillo, C. J. Lim, J. R. Grace and E. J. Anthony, *Energy Fuels*, 2009, **23**, 1437–1444.
40 H. Sun, C. Wu, B. Shen, X. Zhang, Y. Zhang and J. Huang, *Mater. Today Sustain.*, 2018, **1–2**, 1–27.
41 Y. Hu, H. Lu, W. Liu, Y. Yang and H. Li, *Chem. Eng. J.*, 2020, **396**, 125253.
42 J. M. Valverde, *J. Nanopart. Res.*, 2018, **20**, 39.
43 V. Manovic and E. J. Anthony, *Ind. Eng. Chem. Res.*, 2010, **49**, 9105–9110.
44 S. Yang and Y. Xiao, *Ind. Eng. Chem. Res.*, 2008, **47**, 4043–4048.
45 J. Yin, C. Zhang, C. Qin, W. Liu, H. An, G. Chen and B. Feng, *Chem. Eng. J.*, 2012, **198–199**, 38–44.
46 B. Arias, G. S. Grasa and J. C. Abanades, *Chem. Eng. J.*, 2010, **163**, 324–330.
47 A. N. Antzara, A. Arregi, E. Heracleous and A. A. Lemonidou, *Chem. Eng. J.*, 2018, **333**, 697.
48 H. Guo, S. Yan, Y. Zhao, X. Ma and S. Wang, *Chem. Eng. J.*, 2019, **359**, 542–551.
49 J. Sun, W. Wang, Y. Yang, S. Cheng, Y. Guo, C. Zhao, W. Liu and P. Lu, *Fuel*, 2020, **266**, 117056.
50 V. Manovic and E. J. Anthony, *Environ. Sci. Technol.*, 2008, **42**, 4170–4174.
51 K. Labus, *Materials*, 2021, **14**, 548.
52 A. H. Soleimanisalim, M. H. Sedghkerdar, D. Karami and N. Mahinpey, *J. Nat. Gas Sci. Eng.*, 2016, **36**, 1056–1061.
53 S. M. Hashemi, D. Karami and N. Mahinpey, *Fuel*, 2020, **269**, 117432.
54 A. Kurlov, A. Armutlulu, F. Donat, A. R. Studart and C. R. Müller, *Ind. Eng. Chem. Res.*, 2019, **59**, 7182–7188.
55 H. Sun, J. Wang, J. Zhao, B. Shen, J. Shi, J. Huang and C. Wu, *Appl. Catal., B*, 2019, **244**, 63–75.
56 M. Vall, J. Hultberg, M. Strømme and O. Cheung, *RSC Adv.*, 2019, **9**, 20273–20280.
57 C. Luo, Y. Zheng, N. Ding, Q. L. Wu and C. G. Zheng, *Chin. Chem. Lett.*, 2011, **22**, 615–618.
58 H. J. Yoon and K. B. Lee, *Chem. Eng. J.*, 2019, **355**, 850–857.
59 K. S. Sultana, D. T. Tran, J. C. Walmsley, M. Rønning and D. Chen, *Ind. Eng. Chem. Res.*, 2015, **54**, 8929–8939.
60 N. Gao, K. Chen and C. Quan, *Fuel*, 2020, **260**, 116411.
61 R. Han, J. Gao, S. Wei, Y. Su and Y. Qin, *J. Mater. Chem. A*, 2018, **6**, 3462–3470.
62 A. Armutlulu, M. A. Naeem, H. J. Liu, S. M. Kim, A. Kierzkowska, A. Fedorov and C. R. Muller, *Adv. Mater.*, 2017, **29**, 1702896.
63 W. Peng, Z. Xu, C. Luo and H. Zhao, *Environ. Sci. Technol.*, 2015, **49**, 8237–8245.
64 W. Liu, H. An, C. Qin, J. Yin, G. Wang, B. Feng and M. Xu, *Energy Fuels*, 2012, **26**, 2751–2767.

65 B. Azimi, M. Tahmasebpoor, P. E. Sanchez-Jimenez, A. Perejon and J. M. Valverde, *Chem. Eng. J.*, 2019, **358**, 679–690.
66 X. Kou, C. Li, Y. Zhao, S. Wang and X. Ma, *Fuel Process. Technol.*, 2018, **177**, 210–218.
67 Y. Wang, W. Zhang, R. Li, W. Duan and B. Liu, *Energy Fuels*, 2016, 1248–1255.
68 A. N. Antzara, A. Arregi, E. Heracleous and A. A. Lemonidou, *Chem. Eng. J.*, 2018, **333**, 697–711.
69 H. Ping and S. Wu, *RSC Adv.*, 2015, **5**, 65052–65057.
70 S. Wang, H. Shen, S. Fan, Y. Zhao, X. Ma and J. Gong, *Chem. Eng. Sci.*, 2015, **135**, 532–539.
71 M. A. Naeem, A. Armutlulu, Q. Imtiaz and C. R. Müller, *ChemPhysChem*, 2017, **18**, 3280.
72 P. Jamrunroj, S. Wongsakulphasatch, A. Maneedaeng, C. K. Cheng and S. Assabumrungrat, *Powder Technol.*, 2019, **344**, 208–221.
73 J. Chen, T. Shi, L. Duan, Z. Sun and E. J. Anthony, *Chem. Eng. J.*, 2020, **393**, 124716.
74 C. Qin, W. Liu, H. An, J. Yin and B. Feng, *Environ. Sci. Technol.*, 2012, **46**, 1932–1939.
75 Z. Zhou, Y. Qi, M. Xie, Z. Cheng and W. Yuan, *Chem. Eng. Sci.*, 2012, **74**, 172–180.
76 C.-H. Huang, K.-P. Chang, C.-T. Yu, P.-C. Chiang and C.-F. Wang, *Chem. Eng. J.*, 2010, **161**, 129–135.
77 M. Olivares-Marín, E. M. Cuerda-Correa, A. Nieto-Sánchez, S. García, C. Pevida and S. Román, *Chem. Eng. J.*, 2013, **217**, 71–81.
78 M. Broda and C. R. Müller, *Fuel*, 2014, **127**, 94–100.
79 X. Yan, Y. Li, X. Ma, J. Zhao, Z. Wang and H. Liu, *New J. Chem.*, 2019, **43**, 5116–5125.
80 L. Huang, Q. Zheng, B. Louis and Q. Wang, *Energy Technol.*, 2018, **6**, 2469–2478.
81 S. Wei, R. Han, Y. Su, J. Gao, G. Zhao and Y. Qin, *Energy Fuels*, 2019, **33**, 5398–5407.
82 Y. Hu, Y. Guo, J. Sun, H. Li and W. Liu, *J. Mater. Chem. A*, 2019, **7**, 20103–20120.
83 B. W. Hwang, J. H. Lim, H. J. Chae, H.-J. Ryu, D. Lee, J. B. Lee, H. Kim, S. C. Lee and J. C. Kim, *Process Saf. Environ. Prot.*, 2018, **116**, 219–227.
84 X. Zhao, G. Ji, W. Liu, X. He, E. J. Anthony and M. Zhao, *Chem. Eng. J.*, 2018, **332**, 216–226.
85 A. Dal Pozzo, A. Armutlulu, M. Rekhtina, P. M. Abdala and C. R. Müller, *ACS Appl. Energy Mater.*, 2019, **2**, 1295–1307.
86 T. Harada and T. A. Hatton, *Chem. Mater.*, 2015, **27**, 8153–8161.
87 J. S. Kwak, K. R. Oh, K. Y. Kim, J. M. Lee and Y. U. Kwon, *Phys. Chem. Chem. Phys.*, 2019, **21**, 20805–20813.
88 J. Ding, C. Yu, J. Lu, X. Wei, W. Wang and G. Pan, *Appl. Energy*, 2020, **263**, 114681.
89 S. Jin, K. Ho and C.-H. Lee, *Chem. Eng. J.*, 2018, **334**, 1605–1613.
90 H. Joo, S. J. Cho and K. Na, *J. CO2 Util.*, 2017, **19**, 194–201.
91 A.-T. Vu, K. Ho, S. Jin and C.-H. Lee, *Chem. Eng. J.*, 2016, **291**, 161–173.
92 L. Wang, Z. Zhou, Y. Hu, Z. Cheng and X. Fang, *Ind. Eng. Chem. Res.*, 2017, **56**, 5802–5812.
93 Y. Yoo, D. Kang, E. Choi, J. Park and I.-S. Huh, *Chem. Eng. J.*, 2019, **370**, 237–250.
94 Y. Guo, C. Tan, P. Wang, J. Sun, W. Li, C. Zhao and P. Lu, *Chem. Eng. J.*, 2020, **379**, 122277.
95 Y.-D. Ding, G. Song, X. Zhu, R. Chen and Q. Liao, *RSC Adv.*, 2015, **5**, 30929–30935.
96 A. Hanif, S. Dasgupta and A. Nanoti, *Ind. Eng. Chem. Res.*, 2016, **55**, 8070–8078.
97 V. A. Tuan and C. H. Lee, *Vietnam J. Chem.*, 2018, **56**, 197–202.
98 P. Li, W. Liu, J. S. Dennis and H. C. Zeng, *ACS Appl. Mater. Interfaces*, 2017, **9**, 9592–9602.
99 P. Li, Y. Lin, R. Chen and W. Li, *Dalton Trans.*, 2020, **49**, 5183–5191.
100 P. Li and H. C. Zeng, *Environ. Sci. Technol.*, 2017, **51**, 12998–13007.
101 H.-H. Lee, J.-C. Lee, Y.-J. Joo, M. Oh and C.-H. Lee, *Appl. Energy*, 2014, **131**, 425–440.
102 H. Cui, Q. Zhang, Y. Hu, C. Peng, X. Fang, Z. Cheng, V. V. Galvita and Z. Zhou, *ACS Appl. Mater. Interfaces*, 2018, **10**, 20611–20620.
103 A. H. Bork, M. Rekhtina, E. Willinger, P. Castro-Fernández, J. Drnec, P. M. Abdala and C. R. Müller, *Proc. Natl. Acad. Sci.*, 2021, **118**, e2103971118.
104 G. Xiao, R. Singh, A. Chaffee and P. Webley, *Int. J. Greenhouse Gas Control*, 2011, **5**, 634–639.
105 A.-T. Vu, Y. Park, P. R. Jeon and C.-H. Lee, *Chem. Eng. J.*, 2014, **258**, 254–264.
106 C. H. Lee, S. Mun and K. B. Lee, *Chem. Eng. J.*, 2014, **258**, 367–373.
107 K. Zhang, X. S. Li, Y. Duan, D. L. King, P. Singh and L. Li, *Int. J. Greenhouse Gas Control*, 2013, **12**, 351–358.
108 S. I. Jo, Y. I. An, K. Y. Kim, S. Y. Choi, J. S. Kwak, K. R. Oh and Y. U. Kwon, *Phys. Chem. Chem. Phys.*, 2017, **19**, 6224–6232.
109 Y. Qiao, J. Wang, Y. Zhang, W. Gao, T. Harada, L. Huang, T. A. Hatton and Q. Wang, *Ind. Eng. Chem. Res.*, 2017, **56**, 1509–1517.
110 Q. Wang, H. H. Tay, Z. Guo, L. Chen, Y. Liu, J. Chang, Z. Zhong, J. Luo and A. Borgna, *Appl. Clay Sci.*, 2012, **55**, 18–26.
111 M. L. T. Trivino, V. Hiremath and J. G. Seo, *Environ. Sci. Technol.*, 2018, **52**, 11952–11959.
112 S. Jin, K.-J. Ko and C.-H. Lee, *Chem. Eng. J.*, 2019, **371**, 64–77.
113 K. K. Han, Y. Zhou, Y. Chun and J. H. Zhu, *J. Hazard. Mater.*, 2012, **203–204**, 341–347.
114 X. Yang, W. Liu, J. Sun, Y. Hu, W. Wang, H. Chen, Y. Zhang, X. Li and M. Xu, *ChemSusChem*, 2016, **9**, 1607–1613.
115 F. Cova, G. Amica, K. Kohopää and M. V. Blanco, *Inorg. Chem.*, 2019, **58**, 1040–1047.
116 H. Wang, J. Zhang, G. Wang, Q. Wang and T. Song, *J. Therm. Anal. Calorim.*, 2018, **133**, 981–989.
117 X. Chen, Z. Xiong, Y. Qin, B. Gong, C. Tian, Y. Zhao, J. Zhang and C. Zheng, *Int. J. Hydrogen Energy*, 2016, **41**, 13077–13085.

118 H. A. Lara-García, O. Ovalle-Encinia, J. Ortiz-Landeros, E. Lima and H. Pfeiffer, *J. Mater. Chem. A*, 2019, **7**, 4153–4164.
119 K. Wang, J. Hong, Z. Zhou, Z. Lin and P. Zhao, *Energy Technol.*, 2019, **7**, 325–332.
120 X. Yang, W. Liu, J. Sun, Y. Hu, W. Wang, H. Chen, Y. Zhang, X. Li and M. Xu, *ChemSusChem*, 2016, **9**, 2480–2487.
121 M. Seggiani, E. Stefanelli, M. Puccini and S. Vitolo, *Chem. Eng. J.*, 2018, **339**, 51–60.
122 N. Gómez-Garduño and H. Pfeiffer, *Thermochim. Acta*, 2019, **673**, 129–137.
123 D. Peltzer, J. Mùnera, L. Cornaglia and M. Strumendo, *Chem. Eng. J.*, 2018, **336**, 1–11.
124 D. Peltzer, J. Múnera and L. Cornaglia, *J. Environ. Chem. Eng.*, 2019, **7**, 102927.
125 N. Togashi, T. Okumura and K. Oh-Ishi, *J. Ceram. Soc. Jpn.*, 2007, **115**, 324–328.
126 M. V. Blanco, K. Kohopää, I. Snigireva and F. Cova, *Chem. Eng. J.*, 2018, **354**, 370–377.
127 E. Bernabé-Pablo, F. Plascencia-Hernández, A. Yañez-Aulestia and H. Pfeiffer, *Chem. Eng. J.*, 2020, **384**, 123291.
128 M. A. Martínez-Cruz, A. Yañez-Aulestia, G. Ramos-Sánchez, M. Oliver-Tolentino, M. Vera, H. Pfeiffer, D. Ramírez-Rosales and I. González, *Dalton Trans.*, 2020, **49**, 4549–4558.
129 A. Yañez-Aulestia, Q. Wang and H. Pfeiffer, *Phys. Chem. Chem. Phys.*, 2020, **22**, 2803–2813.
130 M. W. Gaultois, M. T. Dunstan, A. W. Bateson, M. S. C. Chan and C. P. Grey, *Chem. Mater.*, 2018, **30**, 2535–2543.
131 T. Harada and T. A. Hatton, *J. Mater. Chem. A*, 2017, **5**, 22224–22233.
132 E. Vera, S. García, M. M. Maroto-Valer and H. Pfeiffer, *Adsorption*, 2020, **26**, 781–792.
133 J. Liu, Z. Wang, Z. Wang, J. Song, G. Li, Q. Xu, J. You, H. Cheng and X. Lu, *Phys. Chem. Chem. Phys.*, 2019, **21**, 13135–13143.
134 L. Martínez-dlCruz and H. Pfeiffer, *J. Phys. Chem. C*, 2012, **116**, 9675–9680.
135 G. Ji, M. Z. Memon, H. Zhuo and M. Zhao, *Chem. Eng. J.*, 2017, **313**, 646–654.
136 T. Zhao, E. Ochoa-Fernández, M. Rønning and D. Chen, *Chem. Mater.*, 2007, **19**, 3294–3301.
137 S. Munro, M. Åhlén, O. Cheung and A. Sanna, *Chem. Eng. J.*, 2020, **388**, 124284.
138 C. Zhao, X. Chen and C. Zhao, *Int. J. Greenhouse Gas Control*, 2010, **4**, 655–658.
139 S. C. Lee, H. J. Chae, S. J. Lee, Y. H. Park, C. K. Ryu, C. K. Yi and J. C. Kim, *J. Mol. Catal. B: Enzym.*, 2009, **56**, 179–184.
140 S. C. Lee and J. C. Kim, *Catal. Surv. Asia*, 2007, **11**, 171–185.
141 M. S. Cho, S. C. Lee, H. J. Chae, Y. M. Kwon, J. B. Lee and J. C. Kim, *Process Saf. Environ. Prot.*, 2018, **117**, 296–306.
142 S. Boonprasop, B. Chalermsinsuwan and P. Piumsomboon, *J. Taiwan Inst. Chem. Eng.*, 2018, **88**, 215–225.
143 G. Yang, H. Luo, T. Ohba and H. Kanoh, *Int. J. Chem. Eng.*, 2016, **2016**, 4012967.
144 F. Miccio, A. N. Murri and E. Landi, *Ind. Eng. Chem. Res.*, 2016, **55**, 6696–6707.
145 Q. Yang and Y. S. Lin, *Ind. Eng. Chem. Res.*, 2006, **45**, 6302–6310.
146 Z. Homonnay, K. Nomura, G. Juhász, M. Gál, K. Sólymos, S. Hamakawa, T. Hayakawa and A. Vértes, *Chem. Mater.*, 2002, **14**, 1127–1135.
147 G. Juhasz, Z. o. Homonnay, K. Nomura, T. Hayakawa, S. Hamakawa and A. Vértes, *Solid State Ionics*, 2001, **139**, 219–231.
148 K. Nomura, Y. Ujihira, T. Hayakawa and K. Takehira, *Appl. Catal., A*, 1996, **137**, 25–36.
149 H. Lu, J. P. Kim, S. H. Son and J. H. Park, *Mater. Lett.*, 2011, **65**, 2858–2860.
150 J. Yi, M. Schroeder, T. Weirich and J. Mayer, *Chem. Mater.*, 2010, **22**, 6246–6253.
151 C. Galven, J.-L. Fourquet, E. Suard, M.-P. Crosnier-Lopez and F. Le Berre, *Dalton Trans.*, 2010, **39**, 4191–4197.
152 B. R. Sneha and V. Thangadurai, *J. Solid State Chem.*, 2007, **180**, 2661–2669.
153 F. Fujishiro, K. Fukasawa and T. Hashimoto, *J. Am. Ceram. Soc.*, 2011, **94**, 3675–3678.
154 J. Yi, T. E. Weirich and M. Schroeder, *J. Membr. Sci.*, 2013, **437**, 49–56.
155 M. T. Dunstan, W. Liu, A. F. Pavan, J. A. Kimpton, C. D. Ling, S. A. Scott, J. S. Dennis and C. P. Grey, *Chem. Mater.*, 2013, **25**, 4881–4891.
156 M. T. Dunstan, P. D. Southon, C. J. Kepert, J. Hester, J. A. Kimpton and C. D. Ling, *J. Solid State Chem.*, 2011, **184**, 2648–2654.
157 M. Li, K. Huang, J. A. Schott, Z. Wu and S. Dai, *Microporous Mesoporous Mater.*, 2017, **249**, 34–41.
158 Y. Zhou, K. Yan, Z. Yang, R. A. Bauer, N. Hong and H. Verweij, *ACS Appl. Nano. Mater.*, 2020, **3**, 6654–6663.
159 H. R. Amedi and M. Aghajani, *J. Nat. Gas Sci. Eng.*, 2016, **35**, 695–702.
160 N. Azizi, T. Mohammadi and R. M. Behbahani, *J. Energy Chem.*, 2017, **26**, 454–465.
161 W. Zhu, F. Liu, M. Gou, R. Guo and X. Li, *Green Chem. Eng.*, 2021, **2**, 132–143.
162 W. M. Aframehr, B. Molki, R. Bagheri, P. Heidarian and S. M. Davodi, *Chem. Eng. Res. Des.*, 2020, **153**, 789–805.
163 C. Cazorla, S. A. Shevlin and Z. X. Guo, *J. Phys. Chem. C*, 2011, **115**, 10990–10995.
164 J. Yu, L.-H. Xie, J.-R. Li, Y. Ma, J. M. Seminario and P. B. Balbuena, *Chem. Rev.*, 2017, **117**, 9674–9754.
165 B. Vujic and A. P. Lyubartsev, *Chem. Eng. Sci.*, 2017, **174**, 174–188.
166 X. Huang, J. Lu, W. Wang, X. Wei and J. Ding, *Appl. Surf. Sci.*, 2016, **371**, 307–313.
167 G. Avci, I. Erucar and S. Keskin, *ACS Appl. Mater. Interfaces*, 2020, **12**, 41567–41579.
168 G. Avci, S. Velioglu and S. Keskin, *ACS Appl. Mater. Interfaces*, 2018, **10**, 33693–33706.
169 H. Fang, A. Kulkarni, P. Kamakoti, R. Awati, P. I. Ravikovitch and D. S. Sholl, *Chem. Mater.*, 2016, **28**, 3887–3896.
170 C. Shi, L. Li and Y. Li, *J. CO2 Util.*, 2020, **42**, 101346.